

Late Miocene–Pliocene eclogite facies metamorphism, D'Entrecasteaux Islands, SE Papua New Guinea

B. D. MONTELEONE,^{1*} S. L. BALDWIN,¹ L. E. WEBB,¹ P. G. FITZGERALD,¹ M. GROVE² AND A. K. SCHMITT²

¹Department of Earth Sciences, Syracuse University, Syracuse, NY 13244, USA (bmontele@syr.edu)

²Department of Earth and Space Sciences, University of California, Los Angeles, Los Angeles, CA 90095, USA

ABSTRACT The D'Entrecasteaux Islands of south-eastern Papua New Guinea are active metamorphic core complexes that formed within a region where the plate tectonic regime has transitioned from subduction to rifting. While rapid, post 4 Myr exhumation and cooling of amphibolite and greenschist facies rocks that constitute the footwall of the crustal scale detachment fault system have been previously documented on Fergusson and Goodenough Islands of the D'Entrecasteaux chain, the timing of eclogite facies metamorphism in rocks of the footwall was unknown. Recent work revealed that at least one of the eclogite bodies formed during the Pliocene. We present combined *in situ* ion microprobe U–Pb age analyses of zircon from five variably retrogressed eclogite samples from Fergusson and Goodenough Islands that document Late Miocene–Pliocene (8–2 Ma) eclogite formation on these islands. Textural relationships and zircon–garnet rare earth element partition coefficients indicate that U–Pb ages constrain zircon crystallization under eclogite facies conditions in all samples. Results suggest westward younging of eclogite facies metamorphism from Fergusson to Goodenough Island. Present-day exposure of Late Miocene–Pliocene eclogites requires exhumation rates $> 2.5 \text{ cm yr}^{-1}$.

Key words: eclogite; exhumation rates; Papua New Guinea; rare earth element; U–Pb; zircon.

INTRODUCTION

Eclogite facies rocks, including those preserving coesite- and diamond-bearing assemblages, have been widely documented in regions of former subduction and plate collision. Their existence at the Earth's surface provides compelling evidence that crustal rocks may be subducted to mantle depths and subsequently brought back to the surface. Geochronological and petrological studies of eclogite facies rocks represent the principal tools for elucidating the pressure–temperature–time evolution of these rocks. They also provide information on rates and physical conditions of metamorphic reactions associated with changes in the Earth's crust during deformation at plate boundaries.

Numerous authors have described high-pressure and ultrahigh-pressure (HP and UHP) rocks in collisional belts, including the Qinling–Dabie–Sulu terrane in China (e.g. Wang *et al.*, 1989; Zhang *et al.*, 1995; Hacker *et al.*, 1998; Hirajima & Nakamura, 2003), the Kokchetev Complex of Kazakhstan (e.g. Shatsky *et al.*, 1989a; Korsakov *et al.*, 1998; Theunissen *et al.*, 2000a), the Western Gneiss region of Norway (e.g. Smith, 1984; Griffin *et al.*, 1985; Wain *et al.*, 2000), and the Western Alps in Europe (e.g. Chopin, 1987;

Compagnoni *et al.*, 1995). Overviews of these regions are provided by Ernst & Liou (2000) and Carswell & Compagnoni (2003). Field and structural relationships, petrology and geochronology have provided P – T – t – D constraints for the burial by subduction, HP/UHP metamorphism at depths $> 100 \text{ km}$ and subsequent retrograde metamorphism during the exhumation of these rocks to the surface. Most mafic eclogites from HP/UHP regions occur as sheared lenses that are enclosed within felsic gneiss and/or schist. Because eclogitic rocks are typically variably retrogressed to amphibolite facies mineral assemblages during exhumation, preservation of HP/UHP assemblages tends to be poor.

While the existence of eclogites occurring in the footwall of active metamorphic core complexes exposed on the D'Entrecasteaux Islands has been recognized for decades in the D'Entrecasteaux region (Davies & Warren, 1988, 1992; Hill & Baldwin, 1993), the timing and mechanism of eclogite facies metamorphism had until recently not been well constrained. The occurrence of exhumed eclogites within an active or very recently active crustal-scale detachment system is unprecedented and presents the possibility that the mechanisms and rates for eclogite exhumation can be determined more definitively here than in older regions.

Constraints for the timing of eclogite formation within the D'Entrecasteaux region will contribute significantly to our understanding of the geodynamic

*Present address: B. D. Monteleone, Department of Earth and Space Exploration, Arizona State University, Bateman Physical Sciences Center, Tempe, AZ 85281, USA.

significance of these rocks. If eclogite formation and exhumation can be related temporally to the active plate motions, valuable constraints for their exhumation history can be obtained by determining the ratio of the depth and time at which they formed. Recently, Baldwin *et al.* (2004) employed *in situ* U–Pb ion microprobe dating of zircon and *in situ* trace and rare earth element (REE) analyses on zircon and garnet to constrain the timing of eclogite facies metamorphism at 4.3 ± 0.4 Ma at one locality on Fergusson Island. In this study, similar methods are applied to five variably retrogressed eclogites in order to constrain the timing of eclogite facies metamorphism and rate of subsequent exhumation of these HP metamorphic rocks. Textural relationships between zircon and surrounding mineral assemblages are critical to interpreting metamorphic conditions for zircon crystallization. *In situ* ion microprobe U–Pb analyses were required to determine the timing of eclogite facies metamorphism in these samples given their low abundance and size.

GEOLOGICAL AND TECTONIC SETTING OF SE PAPUA NEW GUINEA

The geology of south-eastern Papua New Guinea (PNG) records tectonic events within the rapidly evolving Pacific–Australian plate boundary zone. On the Papuan Peninsula, the Owen Stanley Fault is a major northward-dipping thrust fault system that separates metamorphic rocks of Australian crustal origin from overlying obducted mafic and ultramafic

crust of the Papuan Ultramafic Belt (PUB) (Davies, 1971; Fig. 1). Davies (1980a) interpreted the juxtaposition of continental crustal rocks beneath overthrust mafic and ultramafic rocks of the PUB to pre-Eocene choking of north-eastward subduction Australian crust and sediments. This obduction event has been studied at the Musa-Kumusi divide, located on the south-eastern Papuan Peninsula ~200 km west of the D’Entrecasteaux Islands (Lus *et al.*, 2004). K/Ar and $^{40}\text{Ar}/^{39}\text{Ar}$ analyses on amphibole from granulites of the PUB ophiolite metamorphic sole indicate cooling following ophiolite obduction at *c.* 58 Ma (Lus *et al.*, 2004; Fig. 1). Goodenough and Fergusson Island eclogites (Davies & Warren, 1988, 1992; Hill *et al.*, 1992), blueschists of the Emo metamorphics on the Papuan Peninsula (Worthing, 1988), and recently documented blueschists within the Prevost Range of Normanby Island (Little *et al.*, 2006) are all thought to have formed within this northward-dipping subduction zone (Fig. 1).

The Woodlark Basin of eastern PNG records evidence for active continental extension that has given way to westward propagating seafloor spreading since *c.* 6 Ma (Fig. 1) (Taylor *et al.*, 1995, 1999; Goodliffe *et al.*, 1997). The D’Entrecasteaux Islands, Goodenough, Fergusson and Normanby Island, are metamorphic core complexes located west of the seafloor spreading centre tip (Fig. 1) (Davies & Warren, 1988; Hill *et al.*, 1992, 1995; Little *et al.*, 2006). Lower plate rocks exposed on Goodenough and Fergusson Islands contain eclogite facies metamorphic rocks interpreted

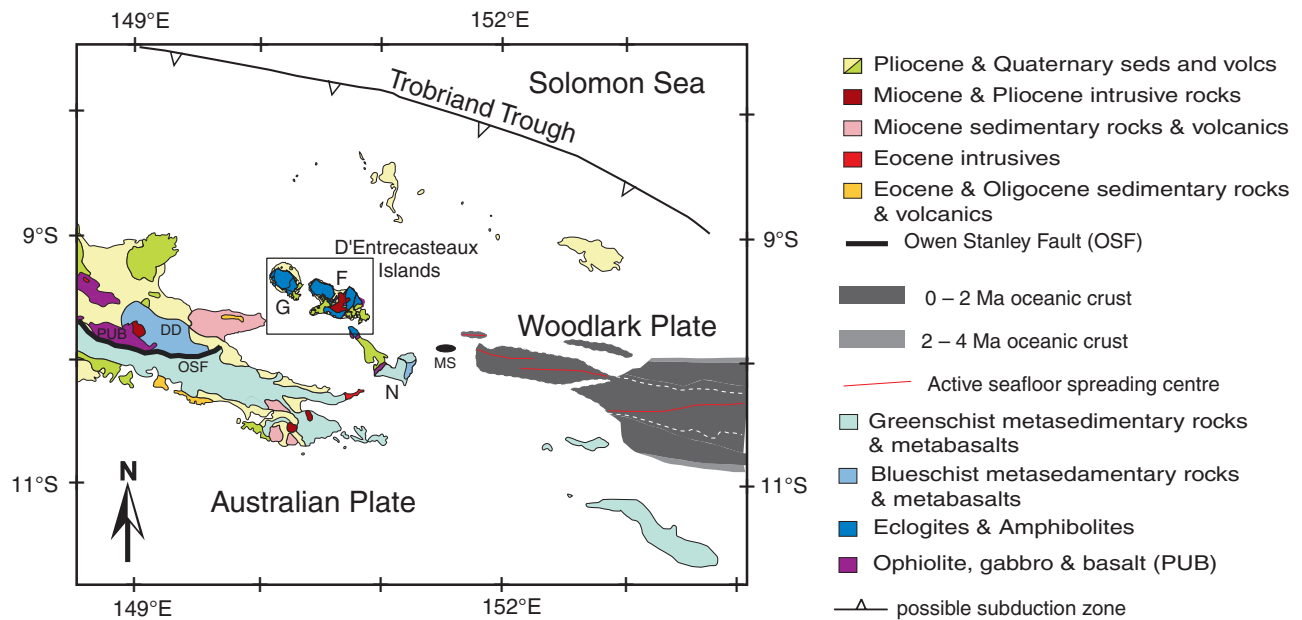


Fig. 1. Simplified tectonic and geological map of south-eastern Papua New Guinea showing major rock units, structures, and the location of the D’Entrecasteaux Islands relative to the (6 Ma–recent) westward propagating seafloor spreading centre (After Davies & Ives, 1965; Davies, 1973; Hill *et al.*, 1992; Baldwin *et al.*, 2004; Little *et al.*, 2006). G = Goodenough Island; F = Fergusson Island, N = Normanby Island; MS = Moresby Seamount; OSF = Owen Stanley Fault; DD = Dayman Dome; PUB = Papuan Ultramafic Belt.

to have been exhumed from beneath predominantly northward-dipping shear zones and detachment faults (Fig. 2) (Hill, 1994). These high-grade metamorphic rocks are juxtaposed against relatively unmetamorphosed ultramafic, volcanic and sedimentary rocks that comprise the hangingwall (Fig. 2) (Davies & Warren, 1988; Baldwin *et al.*, 1993; Hill & Baldwin, 1993).

Previous petrological and thermochronological studies on felsic rocks from the lower plates of Goodenough and Fergusson Islands have documented rapid Pliocene exhumation coincident with the westward propagation of seafloor spreading in the Woodlark Basin (Hill *et al.*, 1992; Baldwin *et al.*, 1993; Hill & Baldwin, 1993; Hill, 1994) (Fig. 1). Thermal histories derived from $^{40}\text{Ar}/^{39}\text{Ar}$ hornblende, biotite, muscovite and K-feldspar step heating experiments from lower plate lithologies are consistent with very recent and very rapid cooling through closure temperatures ranging from ~ 550 to 100 °C during exhumation since < 4 Ma (Baldwin *et al.*, 1993). Similar $^{40}\text{Ar}/^{39}\text{Ar}$

thermochronological studies of felsic shear zone rocks and granodiorite intrusions indicate that syn-tectonic magmatism was coeval with exhumation and cooling of the lower plates since < 4 Ma and provide unequivocal evidence for the close link between magmatism and metamorphic core complex formation (Hill *et al.*, 1995).

Eclogites within lower plates occur as mafic lenses within amphibolite facies felsic gneisses, as mafic dykes cross-cutting felsic gneisses, and as xenoliths within syn-tectonic intrusions. Eclogite facies assemblages consist of garnet + omphacite + rutile \pm SiO_2 \pm phengite \pm kyanite. Retrogressed eclogites contain an amphibolite facies overprint of amphibole (pargasite) + plagioclase + ilmenite \pm titanite (rimming ilmenite) \pm apatite (Fig. 3). Thermobarometry (Ellis & Green, 1979; Gasparik & Lindsley, 1980; Holland, 1980) on a number of samples has provided a wide range of P – T estimates for these eclogites, including: 530 – 840 °C, 12 – 24 kbar (Davies & Warren, 1992); 730 – 900 °C, minimum 21 kbar (Hill & Baldwin, 1993);

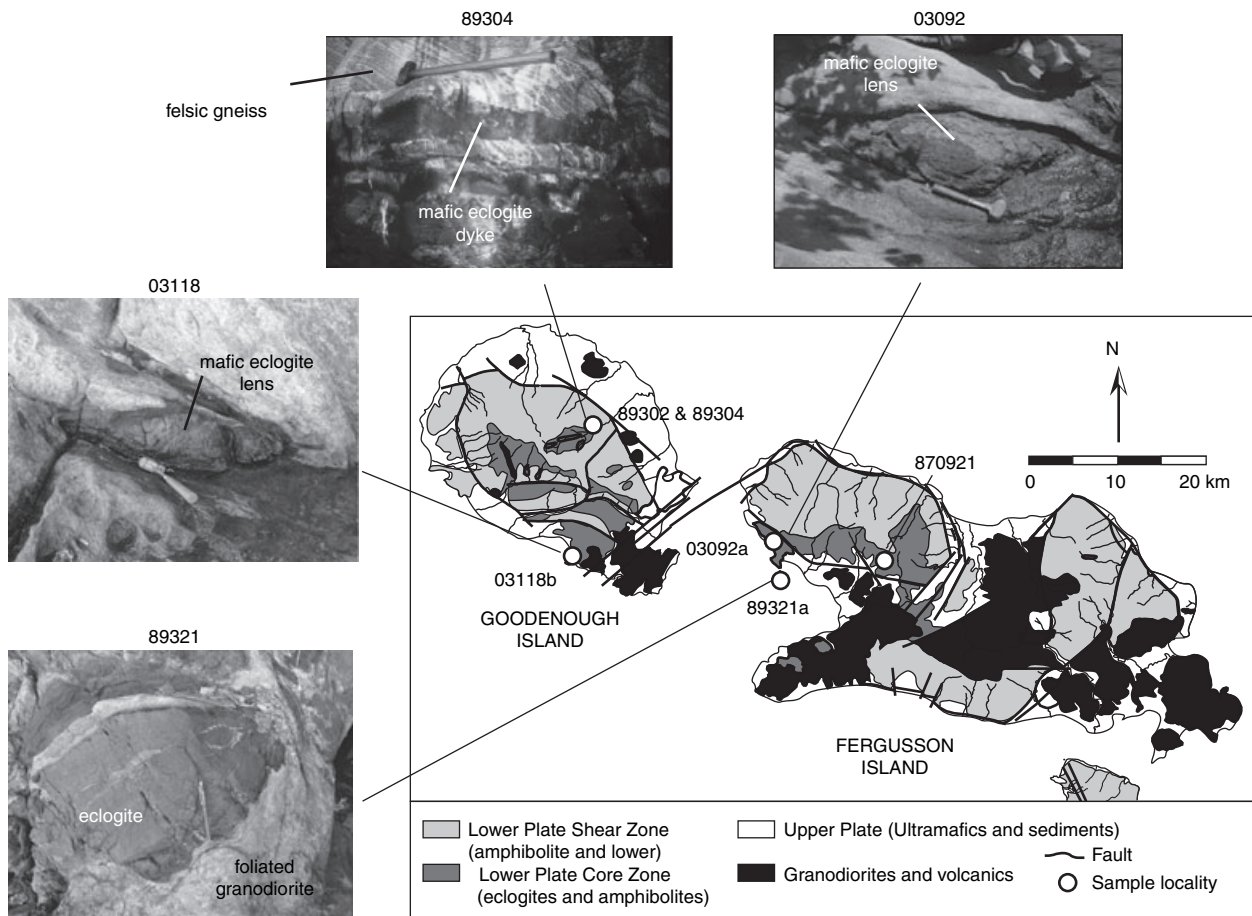


Fig. 2. Simplified map of Goodenough and Fergusson Islands showing areas designated as lower plate shear zone and core zone (after Hill *et al.*, 1992; Baldwin *et al.*, 1993; Hill & Baldwin, 1993; Hill, 1994). Core zones contain mafic eclogites enclosed within felsic gneiss. Sample locations within core zones are indicated along with field photographs. Faults separate lower plate rocks from relatively unmetamorphosed upper plate mafic and ultramafic rocks and sediments. Voluminous granodiorite and felsic to intermediate intrusions occur within the upper and lower plates.

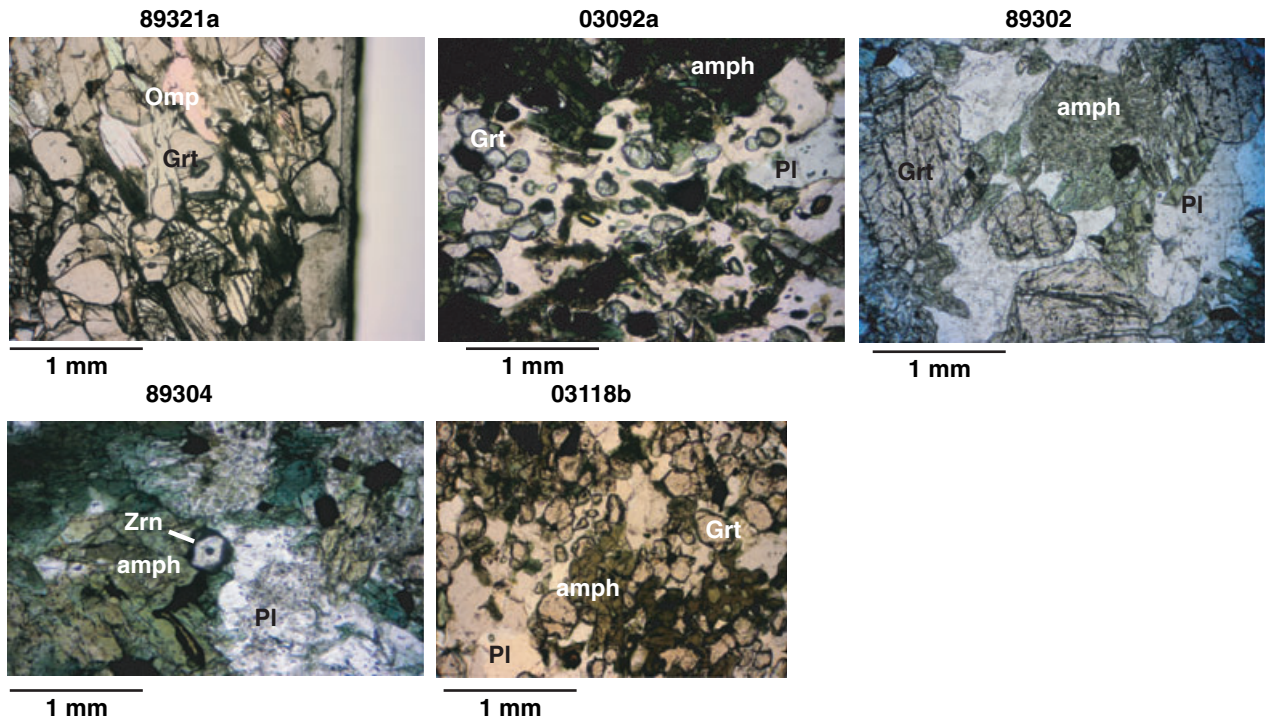


Fig. 3. Photomicrographs of variably retrogressed ecogites from Fergusson and Goodenough Islands. Original ecogite assemblage (garnet + omphacite + quartz + rutile + zircon) is variably retrogressed to amphibolite assemblage in which omphacite and garnet are partially replaced by amphibole + plagioclase (sometimes symplectic), rutile is replaced by ilmenite (occasionally with titanite rims). Sample 89321a is a near pristine ecogite while samples 03092a, 89302 & 89304 preserve only relict garnet + rutile + zircon from ecogite assemblage. Sample 03118b is partially retrogressed, containing omphacite partially replaced by amphibole and plagioclase. Abbreviations from Kretz (1983). Grt = garnet, Zrn = zircon, Omp = omphacite, amph = amphibole, Pl = plagioclase. All photomicrographs taken in plane polarized light.

and 870–930 °C, 20–24 kbar (Baldwin *et al.*, 2004). The range in P – T estimates for these ecogites likely reflects an actual range in P – T conditions recorded by these assemblages, disequilibrium, assumptions made in determination of $\text{Fe}^{2+}/\text{Fe}^{3+}$ ratio (e.g. Ravna, 2000), or a combination thereof. P – T studies of retrograde reactions within enclosing felsic gneiss rocks indicate amphibolite facies retrograde metamorphism within shear zones of 7–11 kbar, 570–730 °C (Hill & Baldwin, 1993).

METHODS

The relatively low modal abundance of zircon, small size (tens of μm), and their occurrence typically as inclusions within garnet frustrated previous efforts to extract zircon from the D'Entrecasteaux Island ecogites using conventional mineral separation techniques. However, recent *in situ* ion microprobe analysis (Baldwin *et al.*, 2004) demonstrated the feasibility of this approach for obtaining U–Pb zircon age constraints for the D'Entrecasteaux Island ecogites. In the present study, five samples were selected from Fergusson and Goodenough Islands (see Appendix 1 for sample descriptions). These include a nearly pristine zircon-bearing ecogite and four variably retrogressed

samples. Evidence for overprinting of ecogite facies mineral assemblages under amphibolite facies conditions includes replacement of omphacite by amphibole and plagioclase and the growth of ilmenite after rutile. All four retrogressed samples contain garnet and rutile interpreted as relicts from the former ecogite facies assemblage. The analytical methods employed to measure zircon U–Pb age and zircon and garnet REE chemistry are described in Appendix 2.

In situ dating of zircon in metamorphic rocks

Thermal Ionization Mass Spectrometry and Secondary Ionization Mass Spectrometry (SIMS) are well-established analytical techniques for determining U–Pb zircon ages. U–Pb dating of zircon in magmatic rocks often provides the timing of crystallization of zircon within a cooling magma chamber, provided that the analysed zircon does not contain an inherited component. In metamorphic rocks, however, interpretation of U–Pb ages obtained on physically separated zircon grains and the relationship between zircon growth and the formation of metamorphic assemblages is not straightforward. Interpretation of U–Pb zircon ages from metamorphic rocks can be hampered by the fol-

lowing factors: (1) the preservation of zircon which leads to inheritance of zircon cores from former igneous or metamorphic events, (2) a poor understanding of how and under what metamorphic conditions zircon crystallization occurs, although mechanisms such as ostwald ripening (e.g. Nemchin *et al.*, 2001; Ayers *et al.*, 2003), crystallization from the breakdown of other Zr-bearing phases (e.g. Bingen *et al.*, 2001; Degeling *et al.*, 2001), and secondary zircon recrystallization (e.g. Pidgeon *et al.*, 1998; Schaltegger *et al.*, 1999) have been proposed, and (3) the relatively low modal abundance and small size of zircon grains within metamorphic rocks.

Zircon grains within metamorphic rocks have traditionally been extracted utilizing conventional mineral separation techniques and their size, shape and zoning characteristics documented by cathodoluminescence (CL) and backscattered electron imaging prior to geochemical and geochronological analysis (e.g. Schaltegger *et al.*, 1999; Warren *et al.*, 2005). Although these methods often produce results that can be interpreted with a high degree of confidence, much debate still exists regarding the nature of zircon growth within multiply deformed and/or highly retrogressed metamorphic rocks. This is because zircon growth may occur during prograde (Rubatto *et al.*, 1999), peak (Rubatto & Hermann, 2003), and retrograde (Brewer *et al.*, 2003; Tomkins *et al.*, 2005) metamorphic conditions.

In situ SIMS analytical techniques have been used successfully to date zircon from metamorphic rocks (e.g. Gebauer, 1996; Vavra *et al.*, 1996; Rubatto *et al.*, 1999; Tomkins *et al.*, 2005). For example, Rubatto *et al.* (1999) successfully employed *in situ* U–Pb dating on zircon inclusions from eclogites of the Sesia-Lanzo

zone of the western Alps. Their study employed CL imaging to define possible zircon growth domains and dated zones from separate eclogite samples throughout the Sesia-Lanzo zone. Further work on Alpine samples by Rubatto (2002), Rubatto & Hermann (2003) and Hermann & Rubatto (2003), along with work by Whitehouse & Platt (2003), demonstrated that *in situ* trace and REE analyses can be used to document contemporaneous equilibrium growth of phases such as zircon and garnet within eclogites and could therefore directly link U–Pb ages of zircon to growth of HP phases (such as garnet) during metamorphism.

RESULTS

Petrology and *P–T* estimates

P–T estimates

Estimation of temperature conditions for eclogite facies metamorphism within these samples required a comprehensive approach utilizing multiple thermometers, including garnet–Cpx Fe–Mg exchange (e.g. Ellis & Green, 1979; Ravna, 2000), [Zr] in rutile (Zack *et al.*, 2004; Watson *et al.*, 2006), and [Ti] in zircon (Watson & Harrison, 2005) thermometry. Results of this comprehensive study are beyond the scope of this paper and will be presented elsewhere. However, a summary of temperature estimates for the samples discussed in this paper are provided in Table 1. Garnet–omphacite thermometry applied to these samples vary as a function of assumed $\text{Fe}^{3+}/\text{Fe}^{2+}$ in omphacite (e.g. Droop, 1987; Ravna & Terry, 2004) and provide temperature estimates with > 300 °C differences within individual samples, thus limiting their use. More precise

Table 1. Summary of location, mineral assemblages, $^{238}\text{U}/^{206}\text{Pb}$ zircon age, and *P–T* constraints for samples from Goodenough and Fergusson Islands.

Sample	Location	Assemblage (s)	$^{238}\text{U}/^{206}\text{Pb}$ age	Eclogite <i>P–T</i>
89321a	9°29'0" S, 150°27'40" E	garnet + omphacite + phengite + rutile + zircon	7.9 ± 1.9 Ma MSWD = 9.2	T_{Zrn} : 650–680 °C T_{RW} : 612–660 °C T_{RZ} : 670–740 °C P_{GCP} : 18–26 kbar P_{jd} : ≥ 15 kbar Coesite present
03092a	9°27'45" S, 150°27'10" E	garnet + rutile + zircon + plagioclase + amphibole + pyrite + ilmenite	7.0 ± 1.0 Ma MSWD = 2.0	T_{RW} : 633–642 °C T_{RZ} : 703–719 °C P_{jd} : no omphacite
89302	9°19'25" S, 150°16'30" E	garnet + rutile + zircon + plagioclase + amphibole + ilmenite	2.94 ± 0.41 Ma MSWD = 1.02	T_{RW} : 718–825 °C T_{RZ} : 828–958 °C P_{jd} : no omphacite
89304	9°19'25" S, 150°16'30" E	garnet + zircon + rutile + plagioclase + amphibole + biotite + pyrite + magnetite + ilmenite	2.82 ± 0.27 Ma MSWD = 2.6	Rutile exsolution in Grt T_{Zrn} : 740–870 °C T_{RW} : 820–880 °C T_{RZ} : 953–1015 °C P_{jd} : no omphacite
03118b	9°29'10" S, 150°14'45" E	garnet + omphacite + rutile + zircon + amphibole + plagioclase + ilmenite	2.09 ± 0.49 Ma MSWD = 3.3	Rutile exsolution in Grt T_{RW} : 677–710 °C T_{RZ} : 771–817 °C P_{jd} : ≥ 14 kbar

T_{Zrn} = temperature from [Ti] in zircon (Watson & Harrison, 2005); T_{RW} = temperature from [Zr] in rutile (Watson *et al.*, 2006); T_{RZ} = temperature from [Zr] in rutile (Zack *et al.*, 2004); P_{jd} = minimum pressure constraint from the jadeite component of omphacite (Gasparik & Lindsley, 1980; Holland, 1980); P_{GCP} = garnet–omphacite–phengite barometry (Ravna & Terry, 2004). The presence of ultrahigh pressure phases (coesite) or possible UHP textures is also indicated.

temperature estimates are obtained by measurement of [Ti] in zircon (samples 89321 and 89304) (Watson & Harrison, 2005) and [Zr] in rutile (all samples) (Zack *et al.*, 2004; Watson & Harrison, 2005). Temperature estimates from [Zr] in rutile (Watson *et al.*, 2006) and [Ti] in zircon (Watson & Harrison, 2005) range from 611 to 870 °C (Table 1). Higher temperature estimates of up to 1015 °C are obtained using the rutile thermometer of Zack *et al.* (2004; Table 1).

Precise determination of pressure conditions for eclogites requires the full assemblage kyanite + phengite + omphacite + garnet (Nakamura & Banno, 1997; Ravna & Terry, 2004). None of the samples in this study contain kyanite, and phengite is present only in sample 89321. Garnet–omphacite–phengite barometry (Ravna & Terry, 2004) for sample 89321 yielded pressure estimates ranging from 18 to 26 kbar for a temperature range of 612–740 °C (Baldwin *et al.*, 2005). The presence of coesite in this sample, however, constrains minimum pressures > 28 kbar, and suggests that the garnet–omphacite–phengite barometry underestimates peak pressures for metamorphism of this sample (Baldwin *et al.*, 2005). Barometry based on the jadeite component of omphacite (Gasparik & Lindsley, 1980) in sample 03118b yields pressures \geq 14 kbar for a temperature range of 677–810 °C (Table 1).

Pressure estimates cannot be determined for samples 03092a, 89302 and 89304. Nonetheless, textural relationships and garnet major element chemistry provide evidence that these rocks may have been metamorphosed under HP, or possibly UHP, conditions (Fig. 3). None of the garnet grains in any retrogressed

samples appear to be in textural equilibrium with retrograde amphibole or plagioclase. Furthermore, with the exception of a few locations where amphibole or plagioclase fills cracks within anhedral and partially replaced garnet grains, garnet does not contain inclusions of retrograde phases. Major element chemistry reveals that garnet grains within samples from this study are unzoned or very weakly zoned, with < 3% total variation in mol.% for Ca, Mg, Fe and Mn (Fig. 4). The lack of zonation in this garnet suggests growth at > 650 °C sufficient for homogenization via volume diffusion (Ghent, 1988). Minor gradients in cation chemistry at grain boundaries (outermost 20 μ m) suggest some diffusion of Ca, Mn, Fe and Mg during retrograde metamorphism. Samples 89321, 03092 and 03118b contain small (< 250 μ m), unzoned to weakly zoned garnet, while samples 89302 and 89304 contain larger garnet grains (250–500 μ m) that are also homogeneous but contain exsolved TiO₂ rods. Although these exsolution features have been attributed to decompression following garnet growth under UHP metamorphic conditions (e.g. Zhang *et al.*, 2003), whether these features necessarily indicate UHP metamorphism is debateable as these features have been documented in granulite facies assemblages (e.g. Page *et al.*, 2003). It should be noted that some samples not included in this study contain garnet cores and rims (e.g. 870921; Baldwin *et al.*, 2004) and felsic gneiss 89303; Hill & Baldwin, 1993). In these samples, exsolved TiO₂ is present in garnet rims but not cores. Overall, textural and compositional characteristics suggest that garnet grains from all samples in this study are a relict phase that had a single growth stage

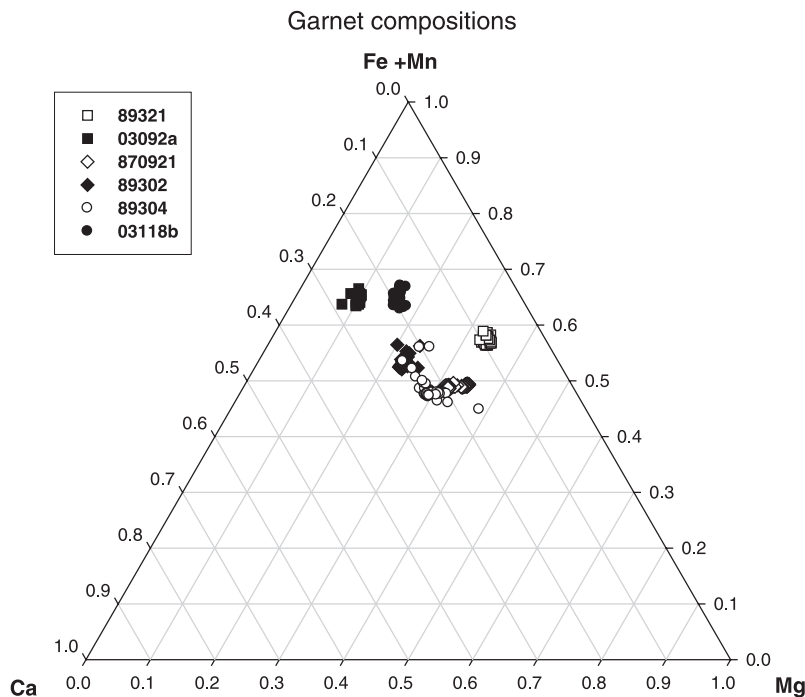


Fig. 4. Ternary diagram plotting compositional data from electron microprobe line transects across garnet grains within samples from this study. Tight clustering of data from individual grains shows that, although garnet compositions differ between samples, samples are generally homogeneous from core to rim.

Table 2. U–Th–Pb data for *in situ* $^{238}\text{U}/^{206}\text{Pb}$ age analyses of zircon from Goodenough and Fergusson Islands.

Analysis	U (ppm)	Th (ppm)	Th/U	$^{204}\text{Pb}/^{206}\text{Pb}$	$^{207}\text{Pb}/^{206}\text{Pb}$	$^{238}\text{U}/^{206}\text{Pb}$	% Radiogenic ^{206}Pb
89321 z11.1	179	43	0.24	0.009 ± 0.002	0.203 ± 0.015	632.91 ± 24.30	83.9 ± 4.1
89321 z11.2	110	11	0.10	0.014 ± 0.004	0.222 ± 0.014	606.06 ± 18.24	73.4 ± 7.0
89321 z11.3	119	13	0.11	0.011 ± 0.003	0.248 ± 0.017	518.13 ± 17.67	79.1 ± 6.2
89321 z13.1	170	25	0.15	0.021 ± 0.004	0.321 ± 0.017	359.71 ± 16.87	60.7 ± 7.0
89321 z12.1	193	60	0.31	0.022 ± 0.004	0.283 ± 0.017	649.35 ± 24.68	59.4 ± 8.2
89321 z12.2	146	47	0.32	0.031 ± 0.007	0.471 ± 0.042	411.52 ± 26.91	42.3 ± 12.7
89321 z14.1	393	196	0.50	0.006 ± 0.001	0.119 ± 0.006	636.94 ± 18.28	89.3 ± 2.3
89321 z14.2	147	58	0.40	0.034 ± 0.006	0.411 ± 0.038	442.48 ± 27.08	36.1 ± 10.7
03092 z69.2	368	7	0.02	0.054 ± 0.004	0.801 ± 0.041	22.60 ± 38.28	14.0 ± 5.7
03092 z70.2	220	5	0.02	0.047 ± 0.003	0.762 ± 0.047	46.06 ± 30.47	10.5 ± 6.0
03092 z70.3	548	31	0.06	0.027 ± 0.003	0.371 ± 0.012	205.89 ± 189.71	49.5 ± 6.3
03092 z71.1	287	3	0.01	0.032 ± 0.003	0.491 ± 0.021	450.25 ± 38.68	40.2 ± 5.1
03092 z71.2	330	5	0.02	0.033 ± 0.003	0.414 ± 0.009	492.13 ± 28.27	38.1 ± 4.9
03092 z71.3	349	9	0.03	0.032 ± 0.003	0.507 ± 0.015	373.27 ± 22.39	39.1 ± 4.7
03092 z76.1	146	2	0.01	0.045 ± 0.003	0.700 ± 0.027	254.91 ± 23.72	15.5 ± 6.4
03092 z76.2	277	4	0.01	0.031 ± 0.003	0.542 ± 0.012	373.41 ± 19.98	41.2 ± 5.2
89302 z2.1	70	36	0.51	0.062 ± 0.006	0.885 ± 0.026	33.32 ± 11.66	-17.5 ± 11.5
89302 z2.2	61	34	0.55	0.052 ± 0.003	0.860 ± 0.038	13.39 ± 3.37	2.2 ± 6.2
89302 z1.1	33	24	0.74	0.052 ± 0.005	0.801 ± 0.021	105.15 ± 5.73	1.0 ± 9.3
89302 z1.2	35	25	0.72	0.057 ± 0.005	0.783 ± 0.022	83.89 ± 3.33	-7.5 ± 8.5
89302 z3.1	135	103	0.76	0.052 ± 0.004	0.801 ± 0.030	172.38 ± 15.30	1.6 ± 8.5
89302 z3.2	138	95	0.69	0.057 ± 0.005	0.763 ± 0.020	194.74 ± 19.43	-7.3 ± 9.2
89302 z4.1	55	45	0.81	0.050 ± 0.003	0.845 ± 0.021	53.85 ± 5.93	4.9 ± 6.3
89302 z4.2	40	46	1.15	0.052 ± 0.004	0.838 ± 0.020	59.56 ± 7.08	1.9 ± 7.6
89302 z6.1	41	23	0.54	0.062 ± 0.017	0.595 ± 0.050	863.56 ± 117.62	-17.4 ± 31.7
89302 z6.2	42	25	0.59	0.032 ± 0.019	0.335 ± 0.047	1165.91 ± 99.53	39.9 ± 35.0
89302 z6.3	37	23	0.61	0.045 ± 0.023	0.320 ± 0.059	1491.20 ± 153.74	14.3 ± 43.5
89302 z5.1	38	25	0.67	0.051 ± 0.007	0.816 ± 0.027	119.35 ± 6.49	3.7 ± 13.5
89302 z6.4	35	23	0.66	0.021 ± 0.012	0.301 ± 0.045	1715.27 ± 135.23	60.4 ± 23.0
89304 z1.1	100	94	0.94	0.023 ± 0.009	0.151 ± 0.021	2053.39 ± 124.64	56.1 ± 16.7
89304 z1.3	222	255	1.15	0.002 ± 0.002	0.062 ± 0.010	2145.00 ± 103.66	96.2 ± 3.8
89304 z1.2	243	390	1.61	0.004 ± 0.002	0.065 ± 0.007	2172.97 ± 89.24	92.4 ± 4.4
89304 z1-2	139	137	0.98	0.004 ± 0.002	0.432 ± 0.040	1162.66 ± 64.48	-2.8 ± 26.3
89304 z2-2.2	138	130	0.95	0.000 ± 0.000	0.283 ± 0.022	1278.28 ± 69.28	100.0 ± 0.0
89304 z2.2	135	147	1.09	0.009 ± 0.007	0.063 ± 0.011	2418.96 ± 110.88	83.4 ± 13.7
89304 z3.1	57	64	1.11	0.016 ± 0.008	0.097 ± 0.017	1870.21 ± 97.27	69.4 ± 15.4
89304 z2.3	196	220	1.12	0.000 ± 0.000	0.064 ± 0.011	2440.81 ± 152.93	100.0 ± 0.0
03118 z56	308	14	0.04	0.008 ± 0.004	0.272 ± 0.017	1998.40 ± 196.76	85.8 ± 7.4
03118 z59	285	8	0.03	0.044 ± 0.002	0.800 ± 0.017	70.08 ± 4.27	16.6 ± 4.7
03118 z59.2	334	6	0.02	0.050 ± 0.003	0.726 ± 0.013	105.65 ± 4.40	6.1 ± 5.1
03118 z59.3	283	5	0.02	0.050 ± 0.006	0.741 ± 0.034	643.92 ± 24.94	6.9 ± 11.4
03118 z55	247	5	0.02	0.048 ± 0.004	0.756 ± 0.015	163.93 ± 8.24	9.1 ± 7.3
03118 z59.4	259	5	0.02	0.037 ± 0.004	0.638 ± 0.021	682.59 ± 47.02	29.6 ± 8.0
03118 z59.5	298	6	0.02	0.035 ± 0.004	0.603 ± 0.015	729.93 ± 48.75	34.1 ± 7.8

[U] and [Th] are derived relative to zircon standard AS3.

prior to retrograde amphibolite facies metamorphism. Although omphacite is lacking in some samples, we interpret garnet from all samples to have grown under eclogite facies (and possibly UHP) conditions (Fig. 3).

Zircon U–Pb ages

In situ ion microprobe ^{238}U – ^{206}Pb analyses were conducted on zircon grains from samples exhibiting varying degrees of retrogression from eclogite to amphibolite facies mineral assemblages. Locating small zircon (average size $\sim 20\ \mu\text{m}$) *in situ* was aided by the ion imaging capacity of the ims 1270 instrument. While beam overlap with surrounding phases was unavoidable in some analyses, inserting a narrow ‘field’ aperture reduced contributions from the analysis crater edge by only admitting ions from the centre of the crater into the mass spectrometer. Furthermore, U and Pb in the host phases (i.e. garnet) are negligibly small compared with the signal from zircon. The age concordance between zircon grains smaller than primary beam spot size and

grains larger than primary beam spot size validates this approach (Baldwin *et al.*, 2004). U–Th–Pb data for five samples are presented in Tables 1 & 2 and are illustrated on Tera–Wasserburg plots (Figs 5 & 6). Errors on age calculations for these Miocene–Pliocene zircon are relatively high (up to $\sim 25\%$) due to low radiogenic Pb relative to common Pb. Analyses of zircon grains from five samples yield single age populations for each sample as discussed below, yet calculated zircon ages varied between samples from *c.* 8 to 2 Ma (Table 1). [U], [Th] and Th/U values are listed in Table 2.

Sample 89321a: Nine analyses were conducted on four zircon grains, with repeated ion drilling into grains when possible. This sample is the least retrogressed and contains a predominantly eclogite facies assemblage. Zircon grains analysed occur as inclusions within garnet. *In situ* ion microprobe analyses of these grains yielded a $^{238}\text{U}/^{206}\text{Pb}$ age of $7.9 \pm 1.9\ \text{Ma}$ (2σ ; MSWD = 9.2; Fig. 5; Tables 1 & 2). Although data points on the Tera–Wasserburg plot do not conform to

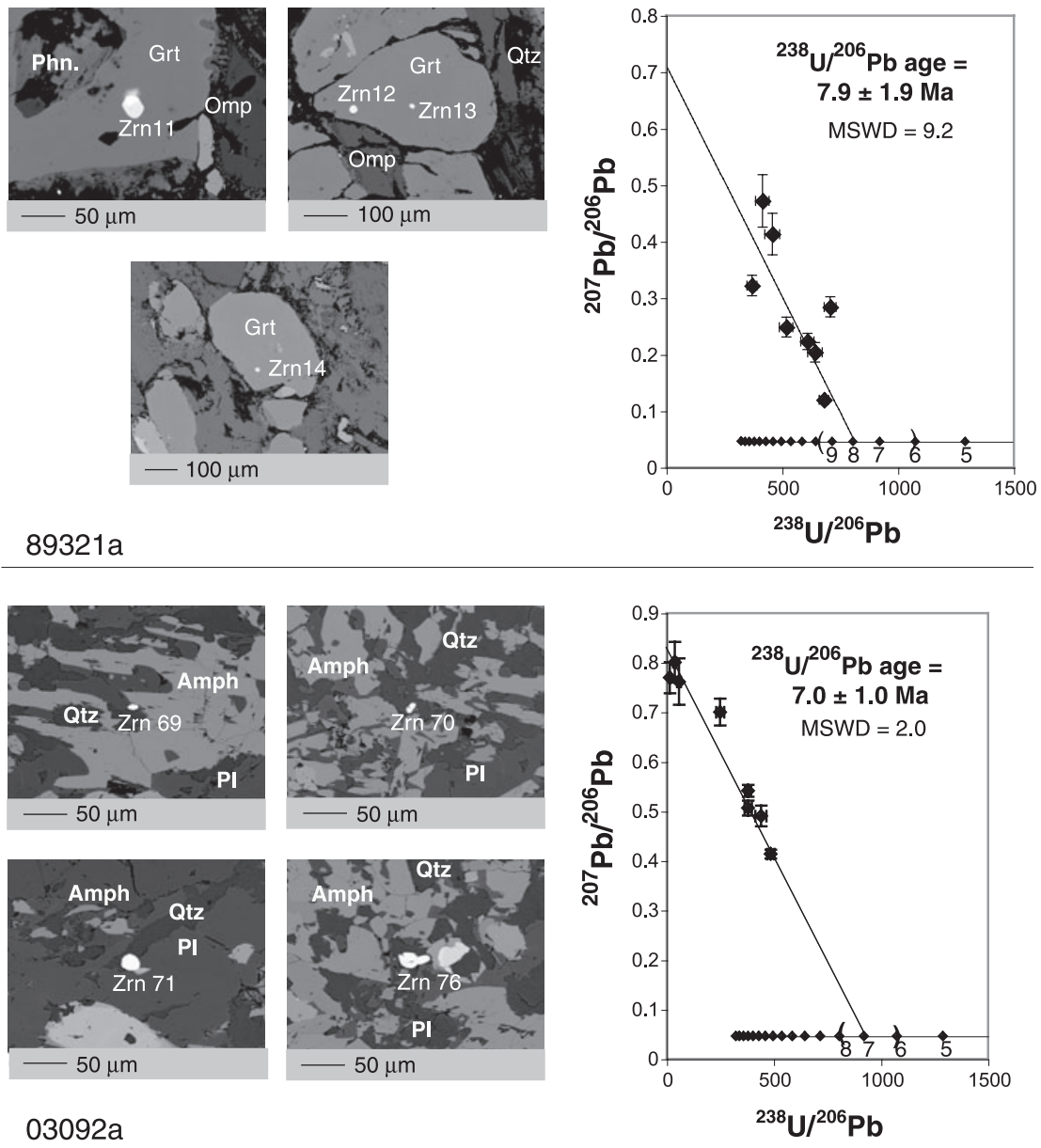


Fig. 5. SEM backscatter images of zircon grains analysed *in situ* for $^{238}\text{U}/^{206}\text{Pb}$ and corresponding Tera-Wasserburg age plots for samples 89321a and 03092a from Fergusson Island. Data are plotted with 1σ error, and brackets on concordia indicate 2σ error on the age regression.

a well-defined line (MSWD = 9.2), a linear regression fit (Mahon, 1996) is used to estimate zircon age based upon all analyses conducted. Due to beam overlap with surrounding garnet, it is possible that some common Pb was contributed by the garnet in addition to the surface-derived common Pb contamination. Therefore, no assumption is made about the common Pb composition in our age regression (i.e. the y -intercept has not been fixed for these analyses, but has been calculated from the best-fit regression line through the data points derived from analyses). Although the high MSWD value suggests the possibility that more than one age

population may be present, we consider efforts to identify multiple populations to be an over-interpretation of these data, given the lack of knowledge of the common Pb composition and the small number of analyses obtained for this sample to date. We note, however, that regression through a pinned $^{207}\text{Pb}/^{206}\text{Pb}$ value of Los Angeles basin anthropogenic lead (0.8283; Sañudo-Wilhelmy & Flegal, 1994) produces an age estimate within error of the unpinned estimate. U and Th concentrations range from 110–393 and 11–196 ppm, respectively. Th/U ranges from 0.1 to 0.5 (Table 2).

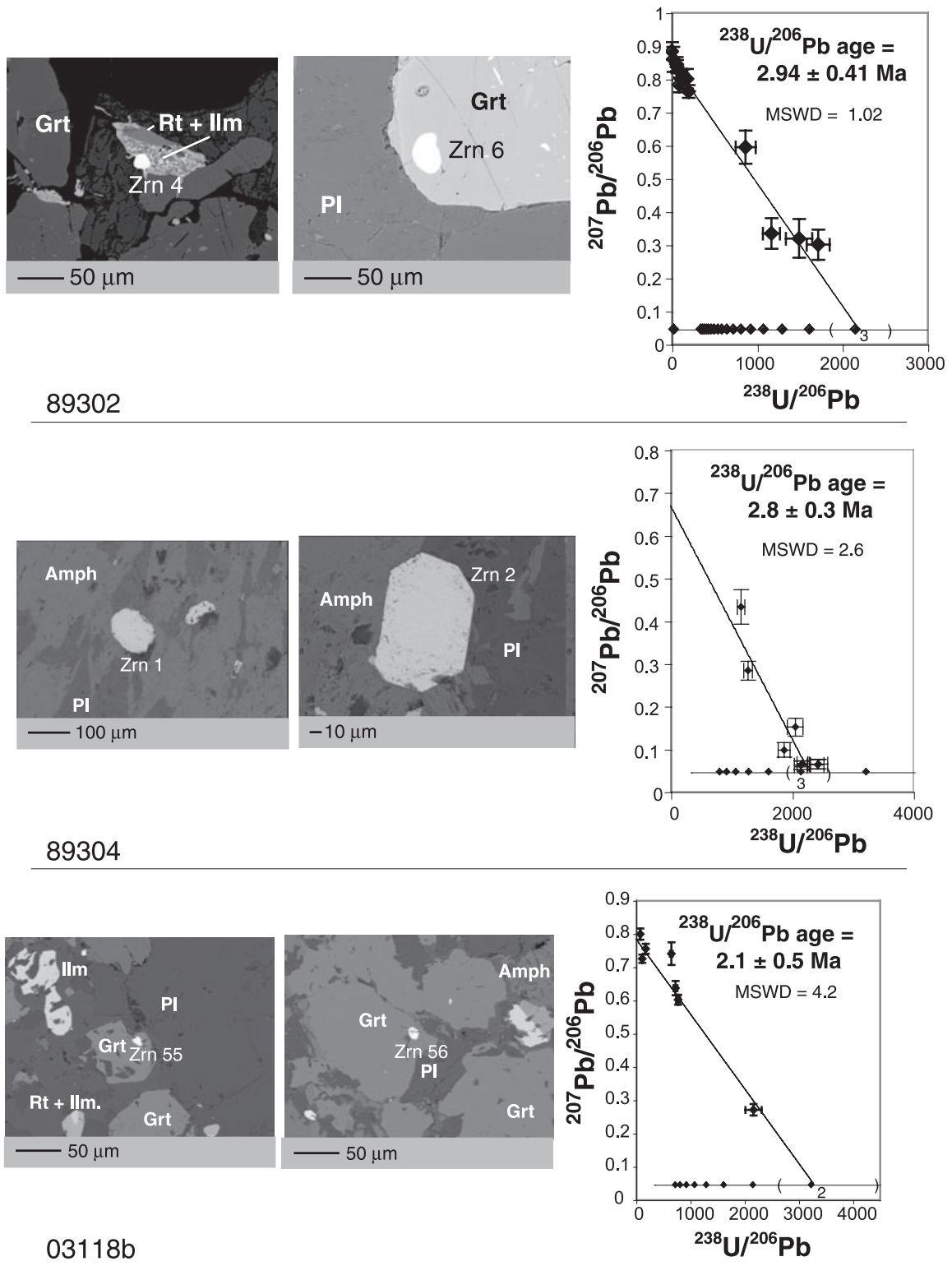


Fig. 6. SEM electron backscatter images of zircon grains analysed *in situ* for $^{238}\text{U}/^{206}\text{Pb}$ and corresponding Tera-Wasserburg age plots for samples 89302, 89304 and 03118b from Goodenough Island. Data are plotted with 1σ error, and brackets on concordia indicate 2σ error on the age regression.

Sample 03092a: Seven analyses were conducted on three zircon grains from sample 03092a. None of the zircon occurs as inclusions within garnet. The small grain size once again made locating and analysing grains challenging. It is possible that adjacent minerals (e.g. garnet, amphibole) were partially included in analyses and assumed in this case to not contribute U or Pb to the analysis. *In situ* ion microprobe analyses of these grains yielded a $^{238}\text{U}/^{206}\text{Pb}$ age of 7.0 ± 1.0 Ma (2σ ; MSWD = 2.0; Fig. 5; Tables 1 & 2). U and Th concentrations range from 146–548 and 2–31 ppm, respectively. Th/U ranges from 0.01 to 0.06 (Table 2).

Sample 89302: Eighteen spot analyses were conducted on six zircon grains from sample 89302. One zircon grain occurs as an inclusion within garnet and five within the amphibole + plagioclase matrix. *In situ* ion microprobe analyses of these grains yielded a $^{238}\text{U}/^{206}\text{Pb}$ age of 2.94 ± 0.41 (2σ ; MSWD = 1.02; Fig. 6; Tables 1 & 2). U and Th concentrations range from 33–138 and 23–103 ppm, respectively. Th/U ranges from 0.5 to 1.1 (Table 2).

Sample 89304: Eight spot analyses were conducted on three zircon grains from sample 89304. These zircon grains occur within the amphibole + plagioclase + biotite matrix. No zircon inclusions were located within garnet, and garnet is largely replaced by retrograde amphibole + plagioclase symplectite. *In situ* ion microprobe analyses of these grains yielded a $^{238}\text{U}/^{206}\text{Pb}$ age of 2.82 ± 0.27 Ma (2σ ; MSWD = 2.6; Fig. 6; Tables 1 & 2). Zircon grains were suitable in size to prevent contamination from outside phases and allowed for multiple spot analyses. Six of the eight spot analyses yielded the most radiogenic analyses among the suite of samples, with uncorrected data that approach concordia, suggesting minimal input of non-radiogenic Pb in this sample and lending confidence to interpretation of this young $^{238}\text{U}/^{206}\text{Pb}$ age. Given the relatively low $^{207}\text{Pb}/^{206}\text{Pb}$ intercept for this sample, the possibility exists that a slightly older age population is also present, but without good constraints on the common Pb component, we prefer to treat these data as a single population. Regression through a pinned $^{207}\text{Pb}/^{206}\text{Pb}$ value of Los Angeles basin anthropogenic lead (0.8283; Sañudo-Wilhelmy & Flegal, 1994) produces an age estimate within error of the unpinned estimate. U and Th concentrations range from 57–243 and 64–390 ppm, respectively. Th/U ranges from 0.9 to 1.6 (Table 2).

Sample 03118b: Seven spot analyses were conducted on three zircon grains within sample 03118b. Zircon grains from sample 03118b occur within the partially retrogressed matrix, which contains relict omphacite, and as inclusions within garnet (Zrn 56). Small zircon grain size (10–15 μm) made ablation of surrounding phases during analyses likely. *In situ* ion microprobe dating of these grains resulted in a $^{238}\text{U}/^{206}\text{Pb}$ age of 2.09 ± 0.49 (2σ ; MSWD = 4.2; Fig. 6; Tables 1 & 2).

Tera-Wasserburg regression on these data included all analyses. U and Th concentrations range from 247–334 and 5–14 ppm respectively. Th/U ranges from 0.02 to 0.04 (Table 2).

In summary, zircon from samples 89321 and 03092a from Fergusson Island have consistent age populations with ages ranging between 8 and 7 Ma. Sample 89321a is a pristine eclogite, while sample 03092a was highly retrogressed under amphibolite facies conditions. Analyses of zircon from three samples from Good-enough Island to the west (89302, 89304 & 03118b) yielded ages from 3 to 2 Ma. Samples 89304 and 89302 from the same locality yielded indistinguishable ages. U–Pb age appears to correlate with location rather than degree of retrograde metamorphism within each sample. Th/U is variable between sample zircon populations. Low Th/U values occur within smaller zircon grains (< 15 μm ; 03092a & 03118b), with higher Th/U occurring within larger zircon grains (89321a, 89302 & 89304).

Trace and REE chemistry

Trace and REE chemical analyses were conducted on zircon and garnet to assess whether zircon growth took place under eclogite facies conditions. A requirement for measuring elemental concentrations of these grains was that grain size of the target mineral exceeded the spot size produced by the primary ion beam, as contribution of surrounding phases to analyses (unlike that for U–Pb analyses described above) would influence derived concentrations. Zircon from samples 89321a and 89304 were suitable for trace and REE concentration analyses, but zircon from 03092a, 89302 and 03118b were too small to obtain ‘non-contaminated’ concentration values. As garnet grain size far exceeded the primary beam spot size, trace and REE concentrations were derived for garnet within all five samples. Garnet grains are relatively homogeneous with the exception of the outer ~ 20 μm within each sample, so analyses were conducted in the homogeneous inner portions of grains. Measured concentrations were normalized to chondritic abundances (McDonough & Sun, 1995). In samples 89321a and 89304, partition coefficients $^{REE}D_{\text{zr/gt}}$ were calculated for comparison to sample 870921a from Fergusson Island (Baldwin *et al.*, 2004) and to other HP/UHP regions (Rubatto & Hermann, 2003; Whitehouse & Platt, 2003).

Samples 89321a and 89304: Trace element and REE analyses of zircon from sample 89321a from Fergusson Island were difficult due to small grain sizes (20–25 μm), however successful analyses were conducted on grains included within garnet. Although the zircon surface appeared sufficiently large to fully contain the primary ion beam spot, some contribution from surrounding garnet grains was unavoidable due to difficulties in exactly locating the primary ion beam on the sample. The garnet contribution, however, was

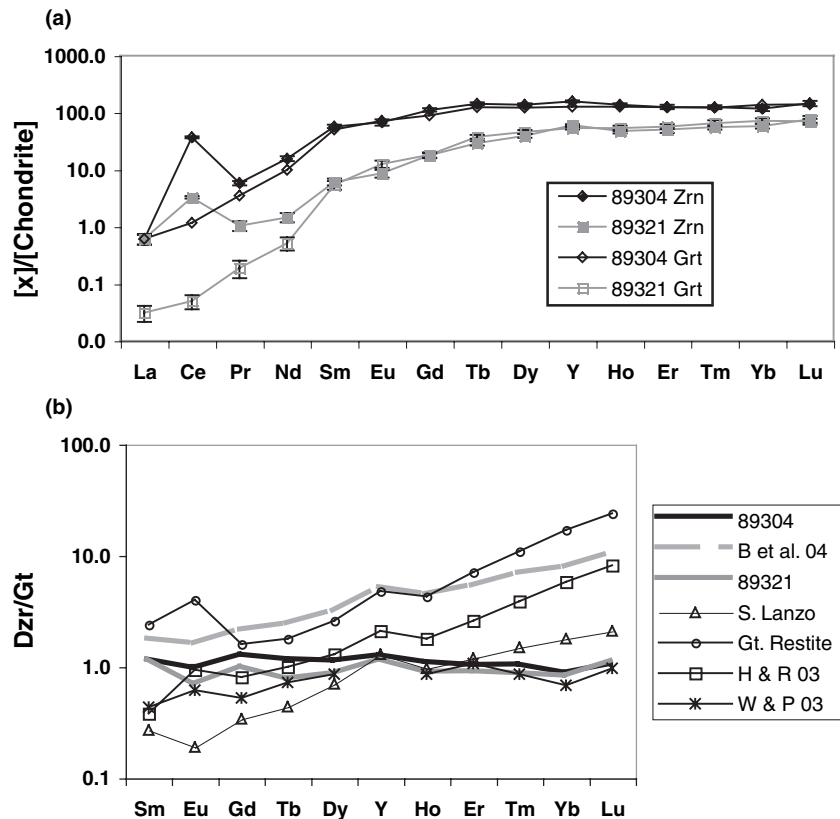


Fig. 7. (a) Chondrite-normalized Y and REE concentrations of zircon and garnet for sample 89321a (Fergusson) and 89304 (Goodenough) (chondrite values from McDonough & Sun, 1995). Data are plotted with 1σ error. (b) $^{REE}D_{zr/gt}$ partition coefficients for samples 89321a and 89304 compared with sample 870921a (B *et al.* 04) (Baldwin *et al.*, 2004), samples from the Western Alps (S. Lanzo, Gt. Restite, H&R 03), (Hermann & Rubatto, 2003; Rubatto & Hermann, 2003), and samples from Spain and Morocco (W&P 03) (Whitehouse & Platt, 2003).

monitored by measuring $^{57}\text{Fe}^+$. A correction was then applied by measuring nearby garnet, and using $^{57}\text{Fe}^+$ in garnet relative to average $^{57}\text{Fe}^+$ in zircon as a proxy for percentage of garnet contamination, subtracting the measured garnet contribution for each element assuming a two-component mixture. This correction was comparable to a second method that used the decrease of $^{91}\text{Zr}^+ / ^{30}\text{Si}^+$ ratio as a proxy for the Si contribution from garnet. Only zircon analyses in which $< 15\%$ garnet contamination occurred were considered adequate for subtraction of garnet contaminant and determination of zircon trace-REE concentration. Plots of chondrite normalized concentrations from zircon grains from sample 89321a yielded a distinct pattern characterized by positive Ce anomaly, absent or very subdued negative Eu anomaly, relative enrichment of middle mass REE (MREE), with subdued enrichment of high mass REE (HREE) (Fig. 7a; Table 3). Zircon grains from sample 89321a are less enriched in MREE relative to other zircon analysed from eclogites from the D'Entrecasteaux Islands. Trace and REE analyses on 89321a garnet yield chondrite-normalized patterns with an absent or subdued negative Eu anomaly, and relatively less enriched HREE (Fig. 7a) (Table 7). Chondrite-normalized concentrations are nearly identical between 89321a zircon and garnet with the exception of light REE (La, Ce, Pr & Nd), which are less abundant in garnet (Fig. 7a) (Table 4).

In situ trace and REE analyses on zircon grains from sample 89304 yielded chondrite-normalized REE patterns with high Ce anomaly, absent negative Eu anomaly, and flattened slope with increasing mass from MREE to HREE (Fig. 7a; Table 4). Chondrite-normalized MREE zircon concentrations are more enriched in 89304 than sample 89321, but the overall pattern is identical to that obtained from sample 870921a from Fergusson Island (Fig. 7a; Baldwin *et al.*, 2004). Chondrite-normalized concentration plots are nearly identical between 89304 zircon and garnet with the exception of light REE (La, Ce, Pr and Nd), which are less abundant in garnet (Fig. 7a). Calculation of $^{REE}D_{zr/gt}$ values yielded nearly identical values between samples 89321a and 89304, with most values plotting near one (Fig. 7b). These values differ from equilibrium values from the western Alps (Hermann & Rubatto, 2003; Rubatto & Hermann, 2003) and sample 870921a from Fergusson Island (Baldwin *et al.*, 2004), which generally plot with increasing $^{REE}D_{zr/gt}$ values with increasing mass (Fig. 7b). However, values derived from 89321a and 89304 are similar to equilibrium values reported by Whitehouse & Platt (2003) (Fig. 7b).

Samples 03092a, 89302 and 03118b: Since zircon grains were too small, trace and REE analyses were conducted only on garnet from these samples. *In situ* ion

Table 3. Trace and REE concentrations and chondrite-normalized concentrations from *in situ* ion microprobe spot analyses on zircon grains.

Zircon REE concentration (ppm)								
Analysis	La ($\pm 1\sigma$)	Ce ($\pm 1\sigma$)	Pr ($\pm 1\sigma$)	Nd ($\pm 1\sigma$)	Sm ($\pm 1\sigma$)	Eu ($\pm 1\sigma$)	Gd ($\pm 1\sigma$)	Tb ($\pm 1\sigma$)
89304z1.1	0.09 \pm 0.01	21.10 \pm 0.12	0.27 \pm 0.01	3.30 \pm 0.05	5.00 \pm 0.07	1.95 \pm 0.03	13.56 \pm 0.22	3.50 \pm 0.06
89304z1.2	0.07 \pm 0.02	18.65 \pm 0.77	0.33 \pm 0.03	2.88 \pm 0.36	3.59 \pm 0.40	1.41 \pm 0.20	7.92 \pm 0.80	1.95 \pm 0.21
89304z1.3	0.14 \pm 0.03	12.69 \pm 0.52	0.21 \pm 0.03	2.55 \pm 0.31	2.81 \pm 0.24	1.49 \pm 0.19	8.29 \pm 0.71	2.39 \pm 0.17
89304z2.3	0.11 \pm 0.02	23.43 \pm 0.94	0.55 \pm 0.05	8.11 \pm 0.90	9.64 \pm 0.72	4.33 \pm 0.51	25.00 \pm 1.68	5.90 \pm 0.38
89304z2.4	0.21 \pm 0.04	22.50 \pm 0.90	0.69 \pm 0.05	10.21 \pm 0.94	11.17 \pm 0.61	5.12 \pm 0.59	29.26 \pm 1.99	6.58 \pm 0.36
89304z2.5	0.20 \pm 0.03	24.38 \pm 0.98	0.78 \pm 0.06	10.69 \pm 0.97	12.20 \pm 0.66	5.68 \pm 0.66	31.98 \pm 2.14	7.09 \pm 0.39
89321z16.1	0.12 \pm 0.02	2.12 \pm 0.11	0.09 \pm 0.02	0.54 \pm 0.13	1.04 \pm 0.17	0.54 \pm 0.08	3.26 \pm 0.35	1.05 \pm 0.09
89321z16.2	0.17 \pm 0.03	1.89 \pm 0.10	0.11 \pm 0.02	1.08 \pm 0.16	0.83 \pm 0.11	0.58 \pm 0.08	3.07 \pm 0.41	1.08 \pm 0.11
89321z17.1	0.15 \pm 0.03	2.13 \pm 0.11	0.09 \pm 0.02	0.64 \pm 0.12	1.05 \pm 0.12	0.54 \pm 0.09	4.06 \pm 0.39	1.19 \pm 0.11
89321z17.2	0.18 \pm 0.04	1.79 \pm 0.10	0.11 \pm 0.02	0.83 \pm 0.14	0.63 \pm 0.09	0.36 \pm 0.06	2.93 \pm 0.35	0.91 \pm 0.07
Analysis	Dy ($\pm 1\sigma$)	Ho ($\pm 1\sigma$)	Er ($\pm 1\sigma$)	Tm ($\pm 1\sigma$)	Yb ($\pm 1\sigma$)	Lu ($\pm 1\sigma$)	Y ($\pm 1\sigma$)	
89304z1.1	24.83 \pm 0.67	5.95 \pm 0.39	16.51 \pm 1.39	2.96 \pm 0.35	17.83 \pm 4.90	3.29 \pm 1.05	208.05 \pm 6.73	
89304z1.2	12.66 \pm 1.32	3.37 \pm 0.41	9.64 \pm 1.32	1.50 \pm 0.21	8.74 \pm 1.28	1.75 \pm 0.34	104.02 \pm 4.59	
89304z1.3	17.70 \pm 1.18	4.33 \pm 0.52	13.99 \pm 1.35	2.40 \pm 0.32	16.44 \pm 1.99	3.11 \pm 0.31	156.03 \pm 6.88	
89304z2.3	38.78 \pm 2.58	8.39 \pm 0.55	20.54 \pm 2.14	3.16 \pm 0.29	19.19 \pm 1.88	3.92 \pm 0.51	312.07 \pm 13.90	
89304z2.4	41.57 \pm 2.12	9.06 \pm 0.60	24.88 \pm 1.77	3.79 \pm 0.24	20.82 \pm 1.60	4.17 \pm 0.34	312.07 \pm 13.90	
89304z2.5	45.90 \pm 2.53	9.60 \pm 0.57	25.75 \pm 1.60	3.98 \pm 0.25	23.64 \pm 1.81	4.27 \pm 0.40	364.08 \pm 16.19	
89321z16.1	10.39 \pm 0.98	2.54 \pm 0.23	6.59 \pm 0.77	1.40 \pm 0.14	9.14 \pm 1.07	1.83 \pm 0.26	93.86 \pm 4.17	
89321z16.2	11.42 \pm 0.87	4.63 \pm 0.69	17.38 \pm 3.71	3.49 \pm 0.83	29.59 \pm 8.59	6.26 \pm 1.67	151.19 \pm 20.15	
89321z17.1	9.90 \pm 0.80	2.66 \pm 0.25	8.95 \pm 1.06	1.48 \pm 0.12	8.66 \pm 0.80	1.96 \pm 0.21	96.41 \pm 4.29	
89321z17.2	8.69 \pm 0.59	2.65 \pm 0.27	8.69 \pm 0.59	1.33 \pm 0.13	10.38 \pm 0.92	1.97 \pm 0.32	94.81 \pm 4.60	
Chondrite normalized zircon REE concentrations								
Analysis	La ($\pm 1\sigma$)	Ce ($\pm 1\sigma$)	Pr ($\pm 1\sigma$)	Nd ($\pm 1\sigma$)	Sm ($\pm 1\sigma$)	Eu ($\pm 1\sigma$)	Gd ($\pm 1\sigma$)	Tb ($\pm 1\sigma$)
89304z1.1	0.38 \pm 0.03	34.42 \pm 0.20	2.86 \pm 0.07	7.22 \pm 0.11	33.76 \pm 0.46	34.90 \pm 0.62	68.15 \pm 1.09	97.26 \pm 1.75
89304z1.2	0.31 \pm 0.02	30.43 \pm 0.77	3.57 \pm 0.03	6.29 \pm 0.36	24.26 \pm 0.40	25.22 \pm 0.20	39.80 \pm 0.80	54.15 \pm 0.21
89304z1.3	0.59 \pm 0.12	20.71 \pm 0.85	2.28 \pm 0.30	5.57 \pm 0.68	18.97 \pm 1.65	26.61 \pm 3.40	41.65 \pm 3.54	66.29 \pm 4.59
89304z2.3	0.48 \pm 0.10	38.23 \pm 1.53	5.96 \pm 0.57	17.74 \pm 1.97	65.14 \pm 4.88	77.28 \pm 9.16	125.61 \pm 8.42	163.91 \pm 10.49
89304z2.4	0.90 \pm 0.15	36.71 \pm 1.47	7.45 \pm 0.58	22.34 \pm 2.06	75.46 \pm 4.10	91.38 \pm 10.54	147.04 \pm 9.98	182.69 \pm 9.89
89304z2.5	0.85 \pm 0.15	39.78 \pm 1.60	8.34 \pm 0.64	23.38 \pm 2.13	82.47 \pm 4.47	101.34 \pm 11.81	160.72 \pm 10.78	196.81 \pm 10.95
89321z16.1	0.49 \pm 0.10	3.45 \pm 0.18	0.96 \pm 0.25	1.18 \pm 0.27	7.03 \pm 1.13	9.70 \pm 1.34	18.22 \pm 1.74	29.15 \pm 2.56
89321z16.2	0.73 \pm 0.14	3.68 \pm 0.16	1.16 \pm 0.17	2.37 \pm 0.35	5.63 \pm 0.73	10.38 \pm 1.41	15.42 \pm 2.03	30.02 \pm 3.11
89321z17.1	0.62 \pm 0.12	3.47 \pm 0.18	1.02 \pm 0.16	1.41 \pm 0.25	7.12 \pm 0.83	9.64 \pm 1.53	20.40 \pm 1.94	32.99 \pm 2.93
89321z17.2	0.75 \pm 0.16	2.92 \pm 0.16	1.14 \pm 0.18	1.82 \pm 0.30	4.27 \pm 0.59	6.48 \pm 0.99	14.70 \pm 1.74	25.23 \pm 1.91
Analysis	Dy ($\pm 1\sigma$)	Ho ($\pm 1\sigma$)	Er ($\pm 1\sigma$)	Tm ($\pm 1\sigma$)	Yb ($\pm 1\sigma$)	Lu ($\pm 1\sigma$)	Y ($\pm 1\sigma$)	
89304z1.1	100.92 \pm 2.72	108.19 \pm 7.11	103.17 \pm 8.71	118.42 \pm 14.04	110.72 \pm 30.46	131.60 \pm 42.17	132.51 \pm 4.28	
89304z1.2	51.47 \pm 1.32	61.31 \pm 0.41	60.24 \pm 1.32	60.07 \pm 0.21	54.31 \pm 1.28	70.01 \pm 0.34	66.26 \pm 4.59	
89304z1.3	71.96 \pm 4.78	78.80 \pm 9.43	87.43 \pm 8.41	96.16 \pm 12.97	102.10 \pm 12.38	124.55 \pm 12.34	99.39 \pm 4.38	
89304z2.3	157.64 \pm 10.50	152.60 \pm 9.93	128.35 \pm 13.35	126.46 \pm 11.46	119.22 \pm 11.69	156.60 \pm 21.21	198.77 \pm 8.85	
89304z2.4	169.00 \pm 8.60	164.75 \pm 10.97	155.52 \pm 11.09	151.61 \pm 9.70	129.31 \pm 9.96	166.68 \pm 13.51	198.77 \pm 8.85	
89304z2.5	186.60 \pm 10.28	174.51 \pm 10.43	160.92 \pm 9.99	159.38 \pm 9.86	146.82 \pm 11.22	170.61 \pm 16.14	231.90 \pm 10.31	
89321z16.1	42.24 \pm 3.99	46.10 \pm 4.19	41.21 \pm 4.83	55.80 \pm 5.78	56.74 \pm 6.64	73.00 \pm 10.48	59.79 \pm 2.65	
89321z16.2	46.41 \pm 3.53	84.16 \pm 12.46	108.60 \pm 23.20	139.57 \pm 33.13	183.80 \pm 53.36	250.32 \pm 66.68	96.30 \pm 12.83	
89321z17.1	40.25 \pm 2.90	48.29 \pm 4.60	55.91 \pm 6.61	59.07 \pm 4.92	53.78 \pm 4.95	78.39 \pm 8.22	61.41 \pm 2.74	
89321z17.2	35.29 \pm 2.38	48.22 \pm 4.89	54.29 \pm 6.22	53.33 \pm 5.02	64.48 \pm 5.71	78.85 \pm 12.78	60.39 \pm 2.93	

Chondrite values from McDonough & Sun (1995). Data are listed with 1σ error.

microprobe analyses yielded concentrations that are consistent within grains and show a distinct pattern when normalized to chondritic meteorite values (McDonough & Sun, 1995). Analyses from all samples yielded chondrite-normalized patterns in which negative Eu anomalies are absent, and MREE, and to a lesser extent HREE, are enriched (Fig. 8). In sample 89302, normalized HREE abundances are lower compared with MREE, thus displaying a negative slope with increasing mass, while normalized garnet MREE and HREE values are similar for other samples (Fig. 8).

DISCUSSION

Eclogites from the lower plates of Fergusson and Goodenough Island occur as mafic dykes, as mafic lenses within enclosing felsic gneiss, and as xenoliths within granodiorite. The mafic protoliths for these eclogites were entrained in northward-subducting felsic crust and sediments derived from the Australian margin prior to peak metamorphism under eclogite facies conditions (Davies & Warren, 1988, 1992; Hill & Baldwin, 1993; Hill, 1994). *In situ* ion microprobe zircon dating and REE chemistry of zircon and garnet

Table 4. Trace and REE concentrations and chondrite-normalized concentrations from *in situ* ion microprobe spot analyses on garnet grains.

Garnet REE concentrations (ppm)								
Analysis	La ($\pm 1\sigma$)	Ce ($\pm 1\sigma$)	Pr ($\pm 1\sigma$)	Nd ($\pm 1\sigma$)	Sm ($\pm 1\sigma$)	Eu ($\pm 1\sigma$)	Gd ($\pm 1\sigma$)	Tb ($\pm 1\sigma$)
89304g1.1	0.17 \pm 0.04	1.30 \pm 0.08	0.51 \pm 0.05	5.48 \pm 0.59	8.24 \pm 0.55	4.11 \pm 0.49	19.69 \pm 1.58	4.48 \pm 0.31
89304g1.2	0.17 \pm 0.04	0.57 \pm 0.09	0.28 \pm 0.03	4.03 \pm 0.45	7.58 \pm 0.63	4.13 \pm 0.50	19.29 \pm 1.41	4.62 \pm 0.34
89304g1.3	0.2 \pm 0.08	1.01 \pm 0.18	0.36 \pm 0.05	4.98 \pm 0.54	8.91 \pm 0.80	4.63 \pm 0.59	20.40 \pm 1.52	5.71 \pm 0.37
89304g2.1	0.12 \pm 0.03	0.54 \pm 0.04	0.25 \pm 0.03	4.20 \pm 0.47	6.69 \pm 0.46	3.59 \pm 0.47	16.41 \pm 1.34	4.08 \pm 0.28
89304g2.2	0.02 \pm 0.01	0.33 \pm 0.03	0.26 \pm 0.03	4.41 \pm 0.50	6.89 \pm 0.54	3.88 \pm 0.47	16.36 \pm 1.30	4.25 \pm 0.27
89304g2.3	0.15 \pm 0.03	0.60 \pm 0.05	0.28 \pm 0.04	4.01 \pm 0.59	6.89 \pm 0.52	3.78 \pm 0.47	15.79 \pm 1.42	4.07 \pm 0.36
89321g17.1	0.03 \pm 0.01	0.07 \pm 0.02	0.03 \pm 0.01	0.28 \pm 0.08	1.39 \pm 0.26	1.02 \pm 0.14	5.00 \pm 0.54	1.64 \pm 0.14
89321g16.1	0.00 \pm 0.00	0.02 \pm 0.01	0.02 \pm 0.01	0.07 \pm 0.04	0.42 \pm 0.09	0.42 \pm 0.08	2.47 \pm 0.29	0.97 \pm 0.09
89321g16.2	0.004 \pm 0.002	0.01 \pm 0.004	0.01 \pm 0.002	0.12 \pm 0.03	0.43 \pm 0.05	0.46 \pm 0.06	2.54 \pm 0.25	1.23 \pm 0.09
89321g18.1	0.002 \pm 0.002	0.01 \pm 0.01	0.01 \pm 0.005	0.19 \pm 0.07	0.55 \pm 0.10	0.58 \pm 0.09	2.96 \pm 0.31	1.27 \pm 0.10
89321g15.1	0.004 \pm 0.003	0.04 \pm 0.01	0.02 \pm 0.01	0.52 \pm 0.10	1.22 \pm 0.20	1.05 \pm 0.15	5.26 \pm 0.56	1.75 \pm 0.14
89302g1.1	0.03 \pm 0.01	0.31 \pm 0.03	0.22 \pm 0.02	4.16 \pm 0.43	11.02 \pm 0.67	4.95 \pm 0.59	21.70 \pm 1.48	4.04 \pm 0.25
89302g3.1	0.04 \pm 0.01	0.38 \pm 0.03	0.26 \pm 0.03	4.80 \pm 0.54	10.31 \pm 0.61	4.70 \pm 0.56	19.95 \pm 1.73	3.62 \pm 0.26
03118bg59.1	0.002 \pm 0.002	0.01 \pm 0.005	0.01 \pm 0.004	0.30 \pm 0.07	1.37 \pm 0.15	1.55 \pm 0.19	9.88 \pm 0.73	3.71 \pm 0.23
03092ag76.1	0.01 \pm 0.004	0.09 \pm 0.01	0.09 \pm 0.01	1.08 \pm 0.17	3.46 \pm 0.27	1.99 \pm 0.24	10.47 \pm 0.78	3.14 \pm 0.19
03092ag76.2	0.04 \pm 0.02	0.08 \pm 0.02	0.05 \pm 0.01	1.14 \pm 0.12	3.79 \pm 0.21	2.30 \pm 0.27	13.48 \pm 0.95	4.29 \pm 0.23
03092ag71.1_2	0.19 \pm 0.06	0.48 \pm 0.12	0.12 \pm 0.02	1.49 \pm 0.17	3.32 \pm 0.23	1.86 \pm 0.22	10.53 \pm 0.71	3.55 \pm 0.20
Analysis	Dy ($\pm 1\sigma$)	Ho ($\pm 1\sigma$)	Er ($\pm 1\sigma$)	Tm ($\pm 1\sigma$)	Yb ($\pm 1\sigma$)	Lu ($\pm 1\sigma$)	Y ($\pm 1\sigma$)	
89304g1.1	30.79 \pm 2.02	6.10 \pm 0.65	16.37 \pm 1.64	2.43 \pm 0.19	14.97 \pm 1.72	2.11 \pm 0.35	173.27 \pm 7.82	
89304g1.2	28.38 \pm 1.52	5.72 \pm 0.41	12.07 \pm 1.34	1.74 \pm 0.24	9.96 \pm 1.50	1.57 \pm 0.26	151.70 \pm 7.09	
89304g1.3	38.35 \pm 2.16	10.05 \pm 0.74	29.30 \pm 2.70	4.82 \pm 0.35	37.59 \pm 3.40	6.13 \pm 0.61	283.73 \pm 13.01	
89304g2.1	28.56 \pm 1.64	7.23 \pm 0.49	22.76 \pm 1.98	3.89 \pm 0.41	25.87 \pm 2.09	4.21 \pm 0.52	217.13 \pm 9.96	
89304g2.2	27.89 \pm 1.98	6.36 \pm 0.47	18.96 \pm 1.74	2.68 \pm 0.29	22.35 \pm 2.45	3.60 \pm 0.36	188.74 \pm 8.37	
89304g2.3	28.22 \pm 1.98	6.55 \pm 0.56	19.93 \pm 1.97	2.96 \pm 0.29	21.46 \pm 1.89	3.50 \pm 0.39	188.98 \pm 8.40	
89321g17.1	13.43 \pm 0.91	3.24 \pm 0.29	10.12 \pm 1.02	1.85 \pm 0.18	12.67 \pm 1.46	1.92 \pm 0.24	92.56 \pm 4.37	
89321g16.1	9.12 \pm 0.80	2.69 \pm 0.44	8.35 \pm 0.83	1.62 \pm 0.24	11.90 \pm 1.30	1.66 \pm 0.22	75.50 \pm 3.65	
89321g16.2	10.47 \pm 0.74	3.11 \pm 0.26	9.87 \pm 0.83	1.87 \pm 0.15	13.53 \pm 1.28	1.89 \pm 0.20	82.79 \pm 4.07	
89321g18.1	11.42 \pm 0.99	2.88 \pm 0.28	9.23 \pm 0.93	1.46 \pm 0.13	10.83 \pm 1.08	1.57 \pm 0.17	84.39 \pm 3.94	
89321g15.1	12.01 \pm 1.07	2.94 \pm 0.34	7.96 \pm 0.89	1.41 \pm 0.20	9.04 \pm 0.90	1.72 \pm 0.23	85.87 \pm 5.70	
89302g1.1	18.40 \pm 1.08	2.61 \pm 0.21	5.54 \pm 0.53	0.75 \pm 0.08	3.34 \pm 0.42	0.67 \pm 0.10	75.73 \pm 3.35	
89302g3.1	16.12 \pm 0.95	2.22 \pm 0.20	4.47 \pm 0.59	0.51 \pm 0.08	3.27 \pm 0.84	0.69 \pm 0.13	67.85 \pm 3.27	
03118bg59.1	28.31 \pm 1.60	6.61 \pm 0.46	16.69 \pm 1.80	2.52 \pm 0.25	14.18 \pm 1.26	2.26 \pm 0.24	168.95 \pm 7.43	
03092ag76.1	24.86 \pm 1.49	6.11 \pm 0.46	16.68 \pm 1.12	2.97 \pm 0.24	22.29 \pm 1.98	3.30 \pm 0.32	183.76 \pm 8.07	
03092ag76.2	33.58 \pm 1.72	8.37 \pm 0.51	23.43 \pm 1.50	3.80 \pm 0.21	28.33 \pm 2.40	4.07 \pm 0.31	239.88 \pm 10.53	
03092ag71.1_2	29.67 \pm 1.49	8.14 \pm 0.51	25.47 \pm 1.69	4.01 \pm 0.26	32.39 \pm 2.43	5.01 \pm 0.49	234.25 \pm 10.27	
Chondrite normalized garnet concentrations								
Analysis	La ($\pm 1\sigma$)	Ce ($\pm 1\sigma$)	Pr ($\pm 1\sigma$)	Nd ($\pm 1\sigma$)	Sm ($\pm 1\sigma$)	Eu ($\pm 1\sigma$)	Gd ($\pm 1\sigma$)	Tb ($\pm 1\sigma$)
89304g1.1	0.72 \pm 0.15	2.12 \pm 0.14	5.50 \pm 0.56	11.99 \pm 1.30	55.69 \pm 3.74	73.39 \pm 8.77	98.95 \pm 7.92	124.57 \pm 8.56
89304g1.2	0.72 \pm 0.18	0.93 \pm 0.15	3.02 \pm 0.36	8.81 \pm 0.99	51.20 \pm 4.26	73.79 \pm 8.98	96.92 \pm 7.10	128.45 \pm 9.38
89304g1.3	0.99 \pm 0.35	1.65 \pm 0.29	3.87 \pm 0.51	10.89 \pm 1.19	60.23 \pm 5.39	82.69 \pm 10.52	102.51 \pm 7.66	158.61 \pm 10.38
89304g2.1	0.51 \pm 0.11	0.87 \pm 0.07	2.73 \pm 0.33	9.19 \pm 1.02	45.22 \pm 3.13	64.06 \pm 8.38	82.45 \pm 6.72	113.42 \pm 7.70
89304g2.2	0.10 \pm 0.04	0.54 \pm 0.06	2.79 \pm 0.34	9.65 \pm 1.09	46.56 \pm 3.66	69.23 \pm 8.38	82.21 \pm 6.52	117.98 \pm 7.53
89304g2.3	0.64 \pm 0.13	0.97 \pm 0.08	3.06 \pm 0.41	8.78 \pm 1.29	46.55 \pm 3.51	67.45 \pm 8.33	79.32 \pm 7.12	112.99 \pm 9.87
89321g17.1	0.11 \pm 0.04	0.11 \pm 0.02	0.34 \pm 0.10	0.62 \pm 0.17	9.40 \pm 1.78	18.22 \pm 2.51	25.12 \pm 2.72	45.50 \pm 3.87
89321g16.1	0.00 \pm 0.00	0.03 \pm 0.01	0.17 \pm 0.07	0.16 \pm 0.08	2.87 \pm 0.58	7.49 \pm 1.38	12.40 \pm 1.45	27.03 \pm 2.54
89321g16.2	0.02 \pm 0.01	0.02 \pm 0.01	0.07 \pm 0.03	0.27 \pm 0.07	2.89 \pm 0.35	8.27 \pm 1.06	12.77 \pm 1.26	34.27 \pm 2.37
89321g18.1	0.01 \pm 0.01	0.02 \pm 0.01	0.11 \pm 0.05	0.42 \pm 0.14	3.75 \pm 0.68	10.28 \pm 1.55	14.87 \pm 1.54	35.24 \pm 2.88
89321g15.1	0.02 \pm 0.01	0.06 \pm 0.02	0.26 \pm 0.08	1.13 \pm 0.23	8.22 \pm 1.32	18.80 \pm 2.66	26.43 \pm 2.82	48.55 \pm 3.94
89302g3.1	0.19 \pm 0.05	0.62 \pm 0.05	2.83 \pm 0.31	10.51 \pm 1.18	69.65 \pm 4.11	83.86 \pm 9.92	100.26 \pm 8.67	100.57 \pm 7.17
03118bg59.1	0.01 \pm 0.01	0.02 \pm 0.01	0.12 \pm 0.04	0.67 \pm 0.16	9.28 \pm 1.04	27.68 \pm 3.32	49.66 \pm 3.67	102.98 \pm 6.26
03092ag76.1	0.04 \pm 0.01	0.15 \pm 0.02	0.96 \pm 0.13	2.37 \pm 0.36	23.39 \pm 1.80	35.60 \pm 4.23	52.60 \pm 3.94	87.31 \pm 5.14
03092ag76.2	0.16 \pm 0.09	0.12 \pm 0.03	0.52 \pm 0.06	2.50 \pm 0.26	25.59 \pm 1.40	41.09 \pm 4.73	67.72 \pm 4.77	119.05 \pm 6.35
03092ag71.1_2	0.82 \pm 0.27	0.78 \pm 0.19	1.33 \pm 0.26	3.27 \pm 0.38	22.42 \pm 1.55	33.13 \pm 3.89	52.91 \pm 3.59	98.50 \pm 5.67
Analysis	Dy ($\pm 1\sigma$)	Ho ($\pm 1\sigma$)	Er ($\pm 1\sigma$)	Tm ($\pm 1\sigma$)	Yb ($\pm 1\sigma$)	Lu ($\pm 1\sigma$)	Y ($\pm 1\sigma$)	
89304g1.1	125.18 \pm 8.20	110.97 \pm 11.90	102.29 \pm 10.26	97.21 \pm 7.63	92.97 \pm 10.69	84.52 \pm 13.92	110.37 \pm 4.98	
89304g1.2	115.37 \pm 6.16	104.06 \pm 7.50	75.42 \pm 8.39	69.71 \pm 9.71	61.89 \pm 9.29	62.70 \pm 10.36	96.63 \pm 4.52	
89304g1.3	155.90 \pm 8.76	182.81 \pm 13.39	183.12 \pm 16.87	192.84 \pm 14.17	233.50 \pm 21.14	245.19 \pm 24.49	180.72 \pm 8.28	
89304g2.1	116.08 \pm 6.67	131.40 \pm 8.84	142.25 \pm 12.37	155.79 \pm 16.58	160.66 \pm 13.01	168.53 \pm 20.73	138.30 \pm 6.35	
89304g2.2	113.38 \pm 8.06	115.69 \pm 8.50	118.49 \pm 10.87	107.01 \pm 11.51	138.79 \pm 15.23	144.19 \pm 14.45	120.22 \pm 5.33	
89304g2.3	114.73 \pm 8.03	119.16 \pm 10.24	124.55 \pm 12.29	118.59 \pm 11.63	133.26 \pm 11.73	139.82 \pm 15.73	120.37 \pm 5.35	
89321g17.1	54.57 \pm 3.68	58.96 \pm 5.29	63.27 \pm 6.39	73.80 \pm 7.22	78.72 \pm 9.10	76.83 \pm 9.58	58.96 \pm 2.78	
89321g16.1	37.08 \pm 3.25	48.85 \pm 8.02	52.22 \pm 5.19	64.94 \pm 9.76	73.91 \pm 8.10	66.55 \pm 8.82	48.09 \pm 2.33	
89321g16.2	42.56 \pm 3.00	56.59 \pm 4.65	61.71 \pm 5.20	74.99 \pm 6.19	84.07 \pm 7.95	75.80 \pm 8.14	52.73 \pm 2.59	
89321g18.1	46.42 \pm 4.01	52.32 \pm 5.07	57.70 \pm 5.80	58.38 \pm 5.33	67.25 \pm 6.69	62.82 \pm 6.65	53.75 \pm 2.51	
89321g15.1	48.83 \pm 4.35	53.44 \pm 6.25	49.76 \pm 5.54	56.51 \pm 7.93	56.13 \pm 5.61	68.79 \pm 9.12	54.69 \pm 3.63	

Table 4 Cont'd

Analysis	Dy ($\pm 1\sigma$)	Ho ($\pm 1\sigma$)	Er ($\pm 1\sigma$)	Tm ($\pm 1\sigma$)	Yb ($\pm 1\sigma$)	Lu ($\pm 1\sigma$)	Y ($\pm 1\sigma$)
89302g3.1	65.52 \pm 3.86	40.33 \pm 3.59	27.93 \pm 3.69	20.28 \pm 3.18	20.30 \pm 5.23	27.51 \pm 5.26	43.22 \pm 2.08
03118bg59.1	115.08 \pm 6.52	120.11 \pm 8.41	104.33 \pm 11.26	100.66 \pm 9.86	88.06 \pm 7.85	90.55 \pm 9.59	107.61 \pm 4.73
03092ag76.1	101.06 \pm 6.06	111.06 \pm 8.28	104.22 \pm 7.02	118.69 \pm 9.65	138.47 \pm 12.28	132.13 \pm 12.60	117.05 \pm 5.14
03092ag76.2	136.51 \pm 6.98	152.26 \pm 9.24	146.44 \pm 9.37	152.19 \pm 8.54	175.96 \pm 14.90	162.73 \pm 12.52	152.79 \pm 6.71
03092ag71.1_2	120.59 \pm 6.07	147.91 \pm 9.28	159.18 \pm 10.55	160.42 \pm 10.55	201.20 \pm 15.10	200.23 \pm 19.74	149.21 \pm 6.54

Chondrite values from McDonough & Sun (1995). Data are listed with 1σ error.

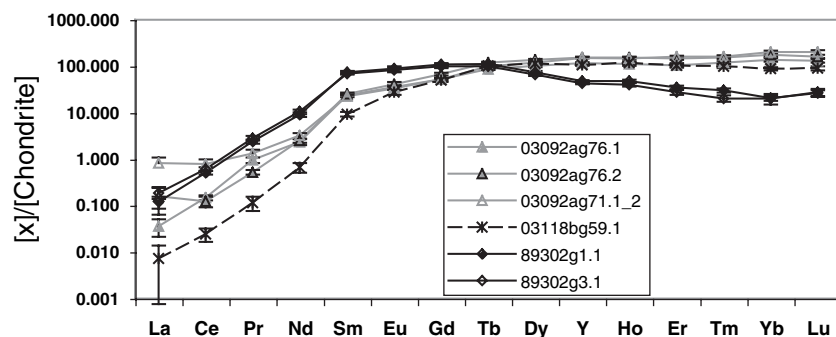


Fig. 8. Chondrite-normalized Y and REE concentrations of garnet from samples 89302, 03092a and 03118b (chondrite values from McDonough & Sun, 1995). Data are plotted with 1σ error.

from retrogressed eclogite sample 870921a documented eclogite facies metamorphism at 4.3 ± 0.4 Ma for one location on Fergusson Island (Fig. 2; Baldwin *et al.*, 2004). *In situ* U–Pb zircon analyses from this study yield a spread of ages from 8 to 2 Ma for five variably retrogressed eclogite samples from Fergusson and Goodenough Islands. It is necessary to use textural relationships between zircon, garnet and the surrounding mineral assemblages along with *in situ* trace and REE analyses of zircon and garnet in order to interpret the significance of these ages with respect to the metamorphic history of these rocks.

Interpretation of U–Pb zircon ages

In situ U–Pb analyses targeted zircon grains from five samples including pristine eclogite (89321a) and retrogressed eclogites (03118b, 03092a, 89302 & 89304). Zircon inclusions in garnet were analysed within samples 89321a, 03118b and 89302, but zircon analysed within 89304 and 03092a were only found within the amphibole and plagioclase matrix.

Inherited zircon is a common feature within many metamorphic rocks. While we cannot completely rule out the possibility that some zircon grains were inherited from other environments or crystallized in the protolith prior to eclogite facies metamorphism, the young age (*c.* 8–2 Ma) of the zircon analysed renders it unlikely that they are inherited. This is especially true given the presence of Archean protoliths in south-eastern PNG (Baldwin & Ireland, 1995). Moreover, it is not feasible to attribute the young age of these zircon populations to Pb loss from inherited zircon grains, given the slow rate of thermally activated diffusion

within zircon under eclogite facies conditions (Cherniak & Watson, 2000).

As zircon grains occur as inclusions within garnet from nearly pristine eclogite sample 89321a, interpretation of zircon growth under eclogite facies conditions for this sample is straight forward. Zircon inclusions in garnet were analysed and are part of single age populations for samples 89302 and 03118b, and as garnet is a relict within the amphibolite facies assemblages, textural evidence supports an interpretation of zircon growth prior to amphibolite facies metamorphism. The case for eclogite facies zircon growth is stronger in 03118b, which also contains omphacite as inclusions in garnet and as a relict phase in the matrix. Although both sample 89304 and 03092a contain garnet as a relict phase within amphibolite facies assemblages, no zircon inclusions were found in garnet. Therefore, textural relationships alone do not rule out zircon growth under amphibolite facies conditions for these samples.

Studies by Rubatto (2002), Rubatto & Hermann (2003), and Hermann & Rubatto (2003), along with work by Whitehouse & Platt (2003) have demonstrated that *in situ* U–Pb age measurement coupled with trace and REE analyses can be used to document contemporaneous growth of phases such as zircon and garnet within eclogites. These pioneering *in situ* studies have shown that it is possible to directly link the growth of zircon to metamorphic assemblages from which *P–T* conditions can be derived. Given the extremely slow diffusion rates for REE within zircon, it can be assumed that measured REE concentrations of zircon represent the concentrations acquired during zircon growth (Cherniak *et al.*, 1997).

As zircon grains within samples 89321 and 89304 were large enough for trace and REE analyses, it is possible to compare trace and REE concentrations from these phases in order to evaluate whether zircon and garnet grew at the same time. The flattened chondrite-normalized HREE patterns measured in zircon from samples 89321a and 89304, coupled with flattened to negative slope of chondrite-normalized HREE patterns in garnet, are consistent with contemporaneous growth of these minerals, (Fig. 8; Rubatto, 2002; Hermann & Rubatto, 2003; Rubatto & Hermann, 2003; Whitehouse & Platt, 2003). The absence of significant negative Eu anomaly in the REE patterns measured from zircon in both samples indicates that plagioclase was absent during zircon growth (Murali *et al.*, 1983; Peucat *et al.*, 1995; Rubatto, 2002). As eclogite assemblages in these samples do not contain plagioclase, but the retrograde amphibolite facies assemblage does contain abundant plagioclase, the lack of Eu anomaly in zircon and garnet implies that contemporaneous growth of these phases occurred under eclogite facies conditions. Zircon–garnet partition coefficients for these samples are nearly identical, but differ from equilibrium values from Baldwin *et al.* (2004), Rubatto & Hermann (2003), and Hermann & Rubatto (2003) which plot with increasing values with increasing REE mass. Values reported in this study have a generally flat slope (~ 1), and are similar to those reported by Whitehouse & Platt (2003). Variation in partition coefficients between samples from this study (89321 & 89304) and sample 870921 from Baldwin *et al.* (2004) (Fig. 8) is due to variable depletion in HREE with increasing mass among garnet from different samples. As trace and REE concentration in garnet may be influenced by other factors (e.g. pressure, temperature, bulk composition; Whitehouse & Platt, 2003), it follows that zircon–garnet partition coefficients may also be dependent on these external factors. The possible influence of these factors on zircon–garnet partition coefficients is currently unknown.

In a similar fashion, the combination of textural relations and trace element and REE analyses of garnet also strongly suggests that zircon from samples 89302 and 03118b grew under eclogite facies conditions. As zircon grains from these samples were smaller than the ion beam spot size, trace element and REE analyses of zircon were not possible. However, the similarity of garnet trace element and REE patterns from these samples (89302 & 03118b) with garnet from samples 89321a and 89304, indicates that garnet from 89302 and 03118b likely grew under similar conditions. The inclusion of some of the analysed zircon grains within garnet in these samples suggests that zircon ages document eclogite facies metamorphism.

The significance of zircon U–Pb age results from sample 03092a is the most difficult to confidently establish. This is because the zircon present within this sample was too small for trace-REE analysis and it

does not occur as inclusions in garnet. Additionally, no omphacite was found in sample 03092a. Nevertheless, garnet Y and REE chemistry are similar to those from other samples, and may therefore indicate growth under similar (eclogite facies) conditions. Specifically, no Eu anomaly was observed and the flattening of chondrite-normalized HREE pattern was similar to all other garnet from this study. Finally, zircon in 03092a has a similar habit (i.e. rounded, unzoned) and U–Pb age as pristine eclogite sample 89321a from a nearby locality.

We conclude that it is most probable that all of the U–Pb zircon ages measured here reflect zircon growth during eclogite facies metamorphism. It is noteworthy that there is no correlation between zircon age and degree of retrograde overprint within samples (i.e. highly retrogressed samples do not preferentially yield the youngest zircon). Instead, variation in zircon age is apparently correlated with location. Zircon U–Pb ages measured for Fergusson Island eclogite samples 89321a (7.9 ± 1.9 Ma) and 03092a (7.0 ± 1.0 Ma) agree within error (Table 2). Both are older than a previously published result (4.3 ± 0.4 Ma) that was obtained from a different location on Fergusson Island (870921a; Baldwin *et al.*, 2004). U–Pb zircon ages for eclogite samples from Goodenough Island cluster even more closely. Samples 89302 (2.94 ± 0.41) and 89304 (2.82 ± 0.27 Ma), located in close proximity to each other (within 1 km), yielded U–Pb ages within error, and are also within 2σ error of sample 03118b (2.09 ± 0.49 Ma) from a different location on Goodenough Island (Fig. 2).

Relationship between mafic eclogites and surrounding felsic gneiss

Mafic eclogites are enclosed by felsic gneiss units that preserve lower pressure assemblages within the lower plates of metamorphic core complexes on Goodenough and Fergusson Islands (Davies & Warren, 1992; Hill & Baldwin, 1993). Sample 89304 is from a mafic intrusion in felsic gneiss. It has been subsequently metamorphosed under eclogite facies conditions, and then partially to completely retrogressed during exhumation. This cross-cutting relationship has been interpreted previously to suggest that surrounding felsic gneiss had also been subjected to eclogite facies P – T conditions, although no eclogite assemblages have yet been documented in these felsic rocks (Hill & Baldwin, 1993). Samples 89301 and 89303 (analyses in Baldwin & Ireland, 1995) are host felsic gneisses for mafic eclogite samples 89302 and 89304 (this study). Unlike the mafic samples examined here, the felsic gneiss samples analysed by Baldwin & Ireland (1995) contained both older, inherited zircon that yielded U–Pb ages up to 96 Ma and youngest zircon populations that yielded U–Pb ages of 2.63 ± 0.16 Ma (2σ) and 2.72 ± 0.26 Ma (2σ) for samples 89301 and 89303. Baldwin & Ireland (1995)

interpreted these young zircon ages to reflect zircon growth during retrograde metamorphism, but alternatively suggested that zircon may have grown during peak or HP metamorphic conditions. Age concordance between zircon from mafic intrusions (89302 & 89304; this study) and young zircon populations from enclosing felsic gneiss (89301 & 89303) suggests that young zircon in felsic gneiss samples also grew under eclogite facies conditions. The combined results of our current study and that of Baldwin & Ireland (1995) indicate contemporaneous zircon growth within both mafic eclogites and surrounding felsic gneisses and support structural and field-based interpretations (Hill, 1994) that felsic gneisses also experienced peak P - T conditions at depths corresponding to eclogite facies conditions.

Mechanisms for zircon growth

Understanding the link between zircon growth, eclogite facies metamorphism and tectonic evolution requires knowledge of the mechanism for zircon growth and the rates of eclogite (and zircon) forming reactions. The presence of what we interpret to be a single age population of zircon within each sample suggests rapid and discrete zircon formation at each locality, as a slow reaction rate would be expected to produce a wider spread of ages within a zircon population. The regional spread of ages determined by this study indicates local variability in the timing of these discrete reactions, with zircon apparently forming earlier on Ferguson Island to the east and later on Goodenough Island to the west.

Because prograde assemblages have to be found for prograde metamorphic reactions in eclogites from the D'Entrecasteaux Islands, zircon and eclogite facies prograde reactions are unknown. Zircon can form by a number of processes including: (1) recrystallization of an inherited zircon, (2) dissolution by fluid and reprecipitation, (3) crystallization from a partial melt of rocks containing either zircon or Zr-bearing minerals, (4) and solid state reactions (e.g. Bingen *et al.*, 2001; Degeling *et al.*, 2001). The possible presence of inherited grains in mafic eclogites cannot be ruled out, although none have yet been identified. Nor is it possible to completely rule out recrystallization or partial to full dissolution and reprecipitation. It should be noted, however, that CL images observed for samples 89304 and 89321 are homogenous, and therefore do not suggest multiple stages of zircon growth nor partial recrystallization. No evidence for melting in mafic eclogites has been found, thereby ruling out crystallization from a partial melt as a mechanism for zircon growth. It is also possible that Zr required for zircon growth was contributed by the breakdown of other phases such as amphibole, pyroxene and ilmenite, all of which may contain tens of ppm Zr (Fraser *et al.*, 1997; Bingen *et al.*, 2001; Degeling *et al.*, 2001). While zircon can also form

from the breakdown of garnet (Fraser *et al.*, 1997; Tomkins *et al.*, 2005), this is unlikely for zircon from the D'Entrecasteaux Islands as they occur as inclusions within garnet (Fig. 3). Textural relationships, trace and REE chemistry support the interpretation of zircon growth under eclogite facies conditions, however, it should be noted that Th/U varies from 0.01 to 1.6 between samples. Th/U generally increases with zircon grain size and temperature estimate (Tables 1 & 2). It is unclear whether different Th/U between samples is a function of differences in zircon growth mechanism.

Mechanisms for eclogite formation

Previous studies have established that eclogites, now exhumed from within the lower plates of the D'Entrecasteaux Island MCCs, formed as a result of northward subduction of the thinned Australian continental margin beneath a Palaeocene island arc (Davies, 1980a; Davies & Jacques, 1984; Davies & Warren, 1988). Continental subduction led to obduction of the island arc and oceanic lithosphere. Evidence of this obduction event is preserved on the PUB on the south-eastern Papuan Peninsula (Davies & Jacques, 1984; Fig. 1). The timing of ophiolite obduction at the Musa-Kumusi divide on the south-eastern Papuan Peninsula has been constrained by *c.* 58 Ma K/Ar and $^{40}\text{Ar}/^{39}\text{Ar}$ step heating ages on amphibole from the metamorphic sole of the ophiolite (Lus *et al.*, 2004; Fig. 1). Our age constraints (8–2 Ma) for eclogite facies metamorphism suggest an apparent *c.* 50 Myr time difference between this obduction event on the south-eastern Papuan Peninsula and the formation of eclogites in the D'Entrecasteaux region.

The relationship between ophiolite obduction at *c.* 58 Ma and the formation of 8–2 Ma eclogites remains unclear. The along-strike variation in the timing of continental subduction, rates of continental subduction, and maximum depths attained during continental subduction are largely unconstrained. Although we have determined a maximum age of *c.* 8 Ma for eclogite facies metamorphism within this suite of samples, the residence time at depth prior to the formation of eclogite facies mineral assemblages remains unknown. In the absence of fluids, it is possible for lower pressure assemblages to be preserved metastably at depths corresponding to eclogite facies conditions for tens of millions of years (e.g. Krabbendam *et al.*, 2000; Wain *et al.*, 2001).

It is possible that a sudden change in pressure, temperature or fluid availability allowed eclogite-forming reactions to proceed rapidly at depth. Although the introduction of fluids has been evoked to explain rapid eclogite formation (Austrheim & Engvik, 2000; Ernst & Liou, 2000; Krabbendam *et al.*, 2000; Wain *et al.*, 2001; Bjornerud & Austrheim, 2004; Camacho *et al.*, 2005), mineral assemblages preserved in these eclogites largely lack hydrous phases and evidence for extensive veining.

We are unable to assess the effect of pressure change on eclogite formation given that only minimum pressures could be constrained for most samples. Zircon and rutile temperature estimates (Watson & Harrison, 2005; Watson *et al.*, 2006), however, document an apparent increase in temperature from 611 to 880 °C for eclogite facies metamorphism from *c.* 8 to 3 Ma within these samples (Table 1).

Eclogite facies metamorphism and the timing of zircon growth may be related to an increase in geothermal gradient within previously subducted crust as rifting and seafloor spreading propagated westwards (Taylor *et al.*, 1995, 1999). Previous petrological and thermochronological studies on Fergusson and Goodenough Islands have demonstrated that these rocks underwent isothermal decompression and that intrusion of massive granodiorites accompanied their exhumation (Baldwin *et al.*, 1993; Hill & Baldwin, 1993; Hill *et al.*, 1995). It is proposed that increasing temperatures may have triggered eclogite facies reactions in these rocks at depth during the early stages of rifting within this former collisional suture.

The spread in U–Pb zircon ages, the lack of preservation of prograde assemblages, and absence of definitive pressure constraints complicate efforts to establish and compare *P–T–t–D* paths followed by these samples. This study has determined that eclogite facies metamorphism and associated zircon-forming reactions occurred from 8 to 2 Ma. Whether zircon formed at peak pressures (i.e. at maximum depths attained during subduction) or at peak temperatures (during the onset or earliest stages of exhumation from maximum depths) remains unknown. The youngest U–Pb zircon ages of *c.* 4.3 Ma on Fergusson Island (Baldwin *et al.*, 2004) and *c.* 2.1 Ma on Goodenough Island document minimum age constraints for when rocks currently exposed on the Earth's surface last resided at eclogite facies conditions.

Exhumation rates

The existence of HP and UHP rocks at the Earth's surface that experienced eclogite facies recrystallization at *c.* 8–2 Ma requires remarkably rapid exhumation rates. We place conservative (lower bound) estimates on the rate of exhumation for these samples by using minimum pressure (depth) constraints from omphacite-bearing samples 03118, 89321a and 870921a (Baldwin *et al.*, 2004). Estimates of exhumation rates for sample 870921a (Baldwin *et al.*, 2004) are 1.7 cm yr⁻¹ for vertical exhumation and 3.5–5.1 cm yr⁻¹ for exhumation from beneath a 20–30° dipping shear zone. Sample 03118b from Goodenough Island was at depths greater than ~50 km (> 14 kbar) at *c.* 2.1 Ma, and has thus been exhumed at a minimum (i.e. vertical) exhumation rate of > 2.5 cm yr⁻¹. Sample 89321a underwent eclogite facies metamorphism at *c.* 7.9 Ma. Our peak pressure estimate for the garnet–omphacite–phengite assemblage is ~25 kbar,

corresponding to 85–90 km depths. A minimum vertical exhumation rate from this depth since *c.* 7.9 Ma is 1.1 cm yr⁻¹, although the presence of coesite in this sample suggests that the exhumation rate may have been higher. Note that exhumation rates provided for samples 89321 and 03118 reflect only the vertical component of exhumation and that displacement rates of rocks exhumed from beneath detachment faults would have been higher. High exhumation rates are consistent with rapid isothermal decompression of these lower plate metamorphic cores as described by Hill & Baldwin (1993) and Baldwin *et al.* (1993). Rapid exhumation rates have also been interpreted for other HP/UHP terranes on the basis of application of multiple chronometers and thermobarometric methods. For example, the Dora-Maira UHP unit within the Alps was exhumed at rates of 3.4 cm yr⁻¹ for a major portion of its exhumation path (Rubatto & Hermann, 2001). Exhumation rates > 2.5 cm yr⁻¹, although very fast, are not inconsistent with this rapidly evolving, seismically active region. Exhumation rates in the lower plates of the D'Entrecasteaux Islands are comparable to seafloor spreading rates (4–7 cm yr⁻¹) within the Woodlark Basin (Benes *et al.*, 1994; Tregoning *et al.*, 1997).

CONCLUSIONS

Eclogites from the D'Entrecasteaux Islands preserve evidence for HP metamorphism at depths > 50 km, and under UHP conditions (sample 89321). While the youngest known eclogite had been previously documented at 4.3 Ma on Fergusson Island (Baldwin *et al.*, 2004), this study documents a range in ages (8–2 Ma) for eclogites from Fergusson and Goodenough Islands. Zircon and garnet trace and REE analyses are consistent with coeval growth of these minerals under eclogite facies conditions, and thus U–Pb zircon ages document the youngest HP/UHP terrane currently known to occur at the Earth's surface. These Late Miocene–Pliocene ages associated with eclogite facies metamorphic rocks necessitate rapid exhumation at rates > 2.5 cm yr⁻¹, comparable with seafloor spreading rates within the Woodlark Basin. The decrease in U–Pb zircon ages from Fergusson Island to Goodenough Island, an east to west younging trend, may correlate with the onset of extension in the Woodlark Basin. The formation of eclogite assemblages in mafic rocks just prior to their exhumation may have been triggered by increasing geothermal gradients associated with the westward propagation of the seafloor spreading centre.

ACKNOWLEDGEMENTS

Funding for this study was provided by the Tectonics and Instrumentation and Facilities Programs, Division of Earth Sciences, U.S. National Science Foundation (to SLB and PGF). SLB acknowledges support from

the ADVANCE program, Lamont Doherty Earth Observatory of Columbia University, during preparation of this manuscript. The ion microprobe facility at UCLA is partly supported by a grant from the Instrumentation and Facilities Program, Division of Earth Sciences, National Science Foundation. D. Rhede (GFZ Potsdam) is thanked for providing the synthetic REE-doped glasses. We thank Dr J. Platt and an anonymous reviewer for providing thorough reviews of the manuscript.

REFERENCES

- Austrheim, H. & Engvik, A. K., 2000. Fluid transport, deformation and metamorphism at depth in a collision zone. In: *Ultra-High Pressure Metamorphism and Geodynamics in Collision-Type Orogenic Belts, Final Report of the Task Group III-6 of the International Lithosphere Project International Book Series*, Vol. 4 (eds Ernst, W. G. & Liou, J. G.), pp. 123–137. Bellwether Publishing Ltd, for the Geological Society of America, Columbia, MD.
- Ayers, J. C., DeLaCruz, K., Miller, C. & Switzer, O., 2003. Experimental study of zircon coarsening in quartzite \pm H₂O at 1.0 Gpa and 1000 °C, with implications for geochronological studies of high-grade metamorphism. *American Mineralogist*, **88**, 365–376.
- Baldwin, S. L. & Ireland, T. R., 1995. A tale of two eras: Pliocene–Pleistocene unroofing of Cenozoic and late Archean zircons from active metamorphic core complexes, Solomon Sea, Papua New Guinea. *Geology*, **23**, 1023–1026.
- Baldwin, S. L., Lister, G. S., Hill, E. J., Foster, D. A. & McDougall, I., 1993. Thermochronologic constraints on the tectonic evolution of active metamorphic core complexes, D'Entrecasteaux Islands, Papua New Guinea. *Tectonics*, **12**, 611–628.
- Baldwin, S. L., Monteleone, B., Webb, L. E., Fitzgerald, P. G., Grove, M. & Hill, E. J., 2004. Pliocene eclogite exhumation at plate tectonic rates in eastern Papua New Guinea. *Nature*, **431**, 263–267.
- Baldwin, S. L., Webb, L. E. & Monteleone, B. D., 2005. Late Miocene–Pliocene eclogites of eastern Papua New Guinea: the youngest known HP/UHP terrane on earth. *Mitteilungen Österreichischer Mineral Gesellschaft*, **150**, 16.
- Benes, V., Scott, S. D. & Binns, R. A., 1994. Tectonics of rift propagation into a continental margin: western Woodlark Basin, Papua New Guinea. *Journal of Geophysical Research*, **99**, 4439–4455.
- Bingen, B., Austrheim, H. & Whitehouse, M., 2001. Ilmenite as a source for zirconium during high-grade metamorphism? Textural evidence from the Caledonides of Western Norway and implications for zircon geochronology. *Journal of Petrology*, **42**, 355–375.
- Bjornerud, M. G. & Austrheim, H., 2004. Inhibited eclogite formation: the key to the rapid growth of strong and buoyant Archean continental crust. *Geology*, **32**, 765–768.
- Brewer, T. S., Storey, C. D., Parrish, R. R., Temperley, S. & Windley, B. F., 2003. Grenvillian age decompression of eclogites in the Glenelg-Attadale Inlier, NW Scotland. *Journal of the Geological Society of London*, **160**, 565–574.
- Camacho, A., Lee, J. K., Hensen, B. J. & Braun, J., 2005. Short-lived orogenic cycles and the eclogitization of cold crust by spasmodic hot fluids. *Nature*, **435**, 1191–1196.
- Carswell, D. A. & Compagnoni, R., 2003. *European Mineralogical Union Notes in Mineralogy, Vol. 5: Ultrahigh Pressure Metamorphism*. Eotvos University Press, Budapest, 508 pp.
- Cherniak, D. J. & Watson, E. B., 2000. Pb diffusion in zircon. *Chemical Geology*, **172**, 5–24.
- Cherniak, D. J., Hanchar, J. M. & Watson, E. B., 1997. Rare-earth diffusion in zircon. *Chemical Geology*, **134**, 289–301.
- Chopin, C., 1987. Very-high pressure metamorphism in the western Alps: implications for subduction of continental crust. *Philosophical Transactions of the Royal Society of London*, **321A**, 183–197.
- Compagnoni, R., Hirajima, T. & Chopin, C., 1995. Ultra-high pressure metamorphic rocks in the Western Alps. In: *Ultra-high Pressure Metamorphism* (eds Coleman, R. G. & Wang, X.), pp. 206–243.
- Davies, H. L., 1971. *Peridotite–Gabbro–Basalt Complex in Eastern Papua: An Overthrust Plate of Oceanic Mantle and Crust*. Bureau of Mineral Resources, Geology and Geophysics, Australia, 128 pp.
- Davies, H. L., 1980a. Crustal structure and emplacement of ophiolite in southeastern Papua New Guinea. *Colloques Internationaux du C.N.R.S.*, **272**, 17–33.
- Davies, H. L. & Jacques, A. L., 1984. Emplacement of ophiolite in Papua New Guinea. *Geological Society of London Special Publication*, **13**, 341–350.
- Davies, H. L. & Warren, R. G., 1988. Origin of eclogite-bearing, domed, layered metamorphic core complexes (“core complexes”) in the D'Entrecasteaux Islands, Papua New Guinea. *Tectonics*, **7**, 1–21.
- Davies, H. L. & Warren, R. G., 1992. Eclogites of the D'Entrecasteaux Islands. *Contributions to Mineralogy and Petrology*, **112**, 463–474.
- Degeling, H., Eggins, S. & Ellis, D. J., 2001. Zr budgets for metamorphic reactions, and the formation of zircon from garnet breakdown. *Mineralogical Magazine*, **65**, 749–758.
- Droop, G. T. R., 1987. A general equation for estimating Fe³⁺ in ferromagnesian silicates and oxides from microprobe analyses using stoichiometric criteria. *Mineralogical Magazine*, **51**, 431–435.
- Ellis, D. J. & Green, D. H., 1979. An experimental study of the effect of Ca upon the garnet-clinopyroxene Fe–Mg exchange equilibria. *Contributions to Mineralogy and Petrology*, **71**, 13–22.
- Ernst, W. G. & Liou, J. G., 2000. Overview of UHP Metamorphism and Tectonics in Well-Studied Collisional Orogens. In: *Ultra-High Pressure Metamorphism and Geodynamics in Collision-Type Orogenic Belts, Final Report of the Task Group III-6 of the International Lithosphere Project International Book Series*, Vol. 4 (eds Ernst, W. G. & Liou, J. G.), pp. 3–20. Bellwether Publishing Ltd, for the Geological Society of America, Columbia, MD.
- Fraser, G., Ellis, D. & Eggins, S., 1997. Zirconium abundance in granulite-facies minerals, with implications for zircon geochronology in high-grade rocks. *Geology*, **25**, 607–610.
- Gasparik, T. & Lindsley, D. H., 1980. Phase equilibria at high pressure of pyroxenes containing monovalent and trivalent ions. In: *Pyroxenes, Reviews in Mineralogy* (ed. Prewitt, C. T.), pp. 309–340. Mineralogical Society of America, Washington DC.
- Gebauer, D., 1996. A *P–T–t* path for an (ultra?) high-pressure ultramafic/mafic rock-association and its felsic country-rocks based on SHRIMP-dating of magmatic and metamorphic zircon domains. Example: Alpe Arami (Central Swiss Alps). In: *Earth Processes: Reading the Isotopic Code*, American Geophysical Union, *Geophysical Monograph*, **95**, 309–328.
- Ghent, E. D., 1988. A review of chemical zoning in eclogite garnets. In: *Eclogites and Eclogite-facies Rocks. (Developments in Petrology 12)* (ed. Smith, D. C.), pp. 207–236. Elsevier, Amsterdam.
- Goodliffe, A. M., Taylor, B., Martinez, F., Hey, R., Maeda, K. & Ohno, K., 1997. Synchronous reorientation of the Woodlark Basin spreading system. *Earth and Planetary Science Letters*, **146**, 233–242.
- Griffin, W. L., Austrheim, H., Brastad, K. *et al.*, 1985. High-pressure metamorphism in the Scandinavian Caledonides. In:

- The Caledonide Orogen Scandinavia and Related Areas* (eds Gee, D. G. & Sturt, B. A.), pp. 783–801. Wiley, Chichester.
- Hacker, B. R., Ratschbacher, L., Webb, L., Ireland, T., Walker, D. & Dong, S., 1998. U–Pb zircon ages constrain the architecture of the ultrahigh-pressure Qinling–Dabie orogen, China. *Earth and Planetary Science Letters*, **161**, 2150–2230.
- Hermann, J. & Rubatto, D., 2003. Relating zircon and monazite domains to garnet growth zones: age and duration of granulite facies metamorphism in the Val Malenco lower crust. *Journal of Metamorphic Geology*, **484**, 1–20.
- Hill, E. J., 1994. Geometry and kinematics of shear zones formed during continental extension in eastern Papua New Guinea. *Journal of Structural Geology*, **16**, 1093–1105.
- Hill, E. J. & Baldwin, S. L., 1993. Exhumation of high-pressure metamorphic rocks during crustal extension in the D'Entrecasteaux region: Papua New Guinea. *Journal of Metamorphic Geology*, **11**, 261–277.
- Hill, E. J., Baldwin, S. L. & Lister, G. S., 1992. Unroofing of active metamorphic core complexes in the D'Entrecasteaux Islands, Papua New Guinea. *Geology*, **20**, 907–910.
- Hill, J., Baldwin, S. L. & Lister, G. S., 1995. Magmatism as an essential driving force for formation of active metamorphic core complexes in eastern Papua New Guinea. *Journal of Geophysical Research*, **100**, 10441–10451.
- Hirajima, T. & Nakamura, D., 2003. The Dabie Shan–Sulu Orogen. In: *European Mineralogical Union Notes in Mineralogy, Vol. 5: Ultrahigh Pressure Metamorphism* (eds Carswell, D. A. & Compagnoni, R.), pp. 1105–1144. Eotvos University Press, Budapest.
- Holland, T. J. B., 1980. The reaction albite = jadeite + quartz determined experimentally in the range 600–1200 °C. *American Mineralogist*, **65**, 129–134.
- Korsakov, A. V., Shatsky, V. S. & Sobolev, N. V., 1998. The first finding of coesite in the eclogites of the Kokchetav Massif. *Doklady Rossiya Akademiyi Nauk*, **360**, 77–81 (in Russian), English translation. *Doklady Earth Sciences*: **360**, 469–473.
- Krabbendam, M., Wain, A. & Andersen, T. B., 2000. Pre-Caledonian granulite and gabbro enclaves in the Western Gneiss Region, Norway: indications of incomplete transition at high pressure. *Geological Magazine*, **137**, 235–255. *The American Mineralogist*, **68**, 277–279.
- Little, T. A., Baldwin, S. L., Fitzgerald, P. G. & Monteleone, B., 2006. A young metamorphic core complex on Normanby Island, D'Entrecasteaux Islands, Papua New Guinea: continental rifting processes near the Woodlark spreading ridge. *Tectonics*, in press.
- Lus, W. Y., McDougall, I. & Davies, H. L., 2004. Age of the metamorphic sole of the Papuan Ultramafic Belt ophiolite, Papua New Guinea. *Tectonophysics*, **392**, 85–102.
- Mahon, K. I., 1996. The “new” York regression: application of an improved statistical method to geochemistry. *International Geology Review*, **38**, 293–303.
- McDonough, W. F. & Sun, S. S., 1995. The composition of the Earth. *Chemical Geology*, **120**, 223–253.
- Murali, A. V., Parthasarathy, R., Mahadevan, T. M. & Sankar Das, M., 1983. Trace element characteristics, REE patterns and partition coefficients of zircons from different geological environments – a case study on Indian Zircons. *Geochimica et Cosmochimica Acta*, **47**, 2047–2052.
- Nakamura, D. & Banno, S., 1997. Thermodynamic modeling of sodic pyroxene solid solution and its application in a garnet–omphacite–kyanite–coesite geothermobarometer for UHP metamorphic rocks. *Contributions to Mineralogy and Petrology*, **130**, 93–102.
- Nemchin, A. A., Giannini, L. M., Bodorkos, S. & Oliver, N. H. S., 2001. Ostwald ripening as a possible mechanism for zircon overgrowth formation during anatexis: theoretical constraints, a numerical model, and its application to pelitic migmatites of the Tickalara Metamorphics, northwestern Australia. *Geochimica et Cosmochimica Acta*, **65**, 2771–2787.
- Page, F. Z., Essene, E. J. & Mukasa, S. B., 2003. Prograde and retrograde history of eclogites from the Eastern Blue Ridge, North Carolina, USA. *Journal of Metamorphic Geology*, **21**, 685–698.
- Pearce, N. J. G., Perkins, W. T., Westgate, J. A. *et al.*, 1995. A compilation of new and published major and trace element data for NIST SRM 610 and NIST SRM 612 glass reference materials. *Geostandards Newsletter*, **21**, 115–144.
- Peucat, J. J., Hirata, T. & Nesbitt, R. W., 1995. REE fractionation (ICPMS LASER) evidence in metamorphic zircons during granulite facies metamorphism and anatexis processes. *Terra Abstracts*, **7**, 346.
- Pidgeon, R. T., Nemchin, A. A. & Hitchen, G. J., 1998. Internal structures of zircons from Archaean granites from the Darling Range batholith: implications for zircon stability and the interpretation of zircon U–Pb ages. *Contributions to Mineralogy and Petrology*, **132**, 288–299.
- Ravna, E. K., 2000. The garnet–clinopyroxene Fe²⁺–Mg geothermometer: an updated calibration. *Journal of Metamorphic Geology*, **18**, 211–219.
- Ravna, E. K. & Terry, M. P., 2004. Geothermobarometry of UHP and HP eclogites and schists – an evaluation of equilibria between garnet–clinopyroxene–kyanite–phengite–coesite/quartz. *Journal of Metamorphic Geology*, **22**, 579–592.
- Rubatto, D., 2002. Zircon trace element geochemistry: partitioning with garnet and the link between U–Pb ages and metamorphism. *Chemical Geology*, **184**, 123–138.
- Rubatto, D. & Hermann, J., 2001. Exhumation as fast as subduction? *Geology*, **29**, 3–6.
- Rubatto, D. & Hermann, J., 2003. Zircon formation during fluid circulation in eclogites (Monviso, Western Alps): implications for Zr and Hf budget in subduction zones. *Geochimica et Cosmochimica Acta*, **67**, 2173–2187.
- Rubatto, D., Gebauer, D. & Compagnoni, R., 1999. Dating of eclogite-facies zircons: the age of Alpine metamorphism in the Sesia–Lanzo Zone (Western Alps). *Earth and Planetary Science Letters*, **167**, 141–158.
- Sañudo-Wilhelmy, S. A. & Flegal, A. R., 1994. Temporal variations in lead concentrations and isotopic composition in the Southern California Bight. *Geochimica et Cosmochimica Acta*, **58**, 3315–3320.
- Schaltegger, U., Fanning, M., Gunther, D., Maurin, J. C., Schulmann, K. & Gebauer, D., 1999. Growth, annealing and recrystallization of zircon and preservation of monazite in high-grade metamorphism: conventional and in-situ U–Pb isotope, cathodoluminescence and microchemical evidence. *Contributions to Mineralogy and Petrology*, **134**, 186–201.
- Shatsky, V. S., Sobolev, N. V. & Gilbert, A. E., 1989a. Eclogites of Kokchetav massif. In: *Eclogites and Glaucofan Schists in Folded Belts* (ed. Sobolev, N. V.), pp. 54–83. Novosibirsk, Nauka.
- Smith, D. C., 1984. Coesite in clinopyroxene in the Caledonides and its implications for geodynamics. *Nature*, **310**, 641–644.
- Taylor, B., Goodliffe, A., Martinez, F. & Hey, R., 1995. Continental rifting and initial sea-floor spreading in the Woodlark Basin. *Nature*, **374**, 534–537.
- Taylor, B., Goodliffe, A. M. & Martinez, F., 1999. How continents break up: insights from Papua New Guinea. *Journal of Geophysical Research*, **104**, 7497–7512.
- Theunissen, K., Dobretsov, N. L., Shatsky, V. S., Smirnova, L. & Korsakov, A., 2000a. The diamond-bearing Kokchetav UHP massif in the Northern Kazakhstan: exhumation structure. *Terra Nova*, **12**, 181–187.
- Tomkins, H. S., Williams, I. S. & Ellis, D. J., 2005. In situ U–Pb dating of zircon formed from retrograde garnet breakdown during decompression in Rogaland, SW Norway. *Journal of Metamorphic Geology*, **23**, 201–215.
- Tregoning, P., Lambeck, K., Stolz, A. *et al.*, 1997. Estimation of current plate motions in Papua New Guinea from global positioning system observations. *Journal of Geophysical Research*, **103**, 12181–12203.
- Vavra, D., Gebauer, D., Schmidt, R. & Compston, W., 1996. Multiple zircon growth and recrystallization during polyphase Late Carboniferous to Triassic metamorphism in granulites of

- the Ivrea Zone (Southern Alps): an ion microprobe (SHRIMP) study. *Contributions to Mineralogy and Petrology*, **122**, 337–358.
- Wain, A., Waters, D., Jephcoat, A. & Olijnyk, H., 2000. The high-pressure to ultrahigh-pressure eclogite transition in the Western Gneiss Region, Norway. *European Journal of Mineralogy*, **12**, 667–687.
- Wain, A. L., Waters, D. J. & Austrheim, H., 2001. Metastability of granulites and processes of eclogitisation in the UHP region of western Norway. *Journal of Metamorphic Geology*, **19**, 609–625.
- Wang, X., Liou, J. G. & Mao, H. K., 1989. Coesite-bearing eclogite from the Dabie mountains in central China. *Geology*, **17**, 1085–1088.
- Warren, C. J., Parrish, R. R., Waters, D. J. & Searle, M. P., 2005. Dating the geologic history of Oman's Semail ophiolite: insights from U–Pb geochronology. *Contributions to Mineralogy and Petrology*, **150**, 403–422.
- Watson, E. B. & Harrison, T. M., 2005. Zircon thermometer reveals minimum melt conditions on early Earth. *Science*, **308**, 841–844.
- Watson, E. B., Wark, D. A. & Thomas, J. B., 2006. Crystalization thermometers for zircon and rutile. *Contributions to Mineralogy and Petrology*, **151**, 413–433.
- Whitehouse, M. J. & Platt, J. P., 2003. Dating high-grade metamorphism – constraints from rare-earth elements in zircon and garnet. *Contributions to Mineralogy and Petrology*, **145**, 61–74.
- Wiedenbeck, M. & 29 others, 2004. Further characterization of the 91500 zircon crystal. *Geostandards and Geoanalytical Research*, **28**, 9–39.
- Worthing, M. A., 1988. Petrology and tectonic setting of blueschist facies metabasites from the Emo Metamorphics of Papua New Guinea. *Australian Journal of Earth Sciences*, **35**, 159–168.
- Zack, T., Morales, R. & Kronz, A., 2004. Temperature dependence of Zr in rutile: empirical calibration of a rutile thermometer. *Contributions to Mineralogy and Petrology*, **148**, 471–488.
- Zhang, R. Y., Liou, J. G. & Ernst, W. G., 1995. Ultrahigh pressure metamorphism and decompressional P–T paths of eclogites and country rocks from Weihei, eastern China. *Island Arc*, **4**, 293–309.
- Zhang, R. Y., Zhai, S. M., Fei, Y. W. & Liou, J. G., 2003. Titanium solubility in coexisting garnet and clinopyroxene at very high pressure: the significance of exsolved rutile in garnet. *Earth and Planetary Science Letters*, **216**, 591–601.

Received 25 March 2006; revision accepted 4 May 2006.

APPENDIX 1: SAMPLE DESCRIPTIONS

Fergusson Island

Sample 89321a is a pristine eclogite sample from a mafic xenolith from Tomabaguna Island, located offshore of western Fergusson Island (Fig. 2). The island consists of mafic xenoliths occurring within weakly foliated rocks of granodiorite composition previously interpreted as granodiorite intrusions (Davies & Warren, 1992; Hill & Baldwin, 1993). Although sample 89321a is not retrogressed, the xenolith from which it was sampled contains widespread and variable retrogression to amphibolite facies assemblages (amphibole + plagioclase) on its rind. These xenoliths, containing pristine eclogite pockets among retrograde amphibolites, are in turn enclosed by quartz pegmatites. Sample 89321a contains the assemblage: garnet (almandine) + omphacite + quartz + phengite + rutile + zircon (Fig. 3) (Table 1). Garnet grains have sub-rounded edges and occur in anhedral, often elongated shapes. Zircon grains are rounded, sub-equant, ~15–25 μm in shortest dimension, and occur as inclusions within garnet and within the omphacite (+ minor quartz) matrix.

Sample 03092a is from a mafic lens within lower plate felsic gneiss on the western coast of Fergusson Island (Fig. 2). The sample preserves the assemblage garnet + rutile + quartz + zircon + retrograde amphibole + plagioclase (Fig. 3; Table 1). Zircon analysed from 03092a is rounded and small (~15 μm), and occurs within a matrix of amphibole and plagioclase, interpreted to be retrograde. Very small (< 5 μm) rounded zircon grains also occur as inclusions within rutile-ilmenite intergrowths. Textures provide evidence for ilmenite replacement of former rutile in which zircon grains were included. Garnet grains are < 100 μm and are replaced at rims by amphibole. The matrix is fine grained and includes amphibole, plagioclase and quartz.

Goodenough Island

Sample 89302 is from a mafic lens within felsic gneiss. Sample 89302 contains garnet + rutile + amphibole + plagioclase + quartz (Fig. 3; Table 1). Garnet is up to 500 μm in diameter, rounded, anhedral and highly fractured. This garnet is interpreted to be relict based on replacement by retrograde plagioclase and amphibole within fractures and on garnet rims. Amphibole and plagioclase are

pervasive within the sample matrix. No relict omphacite has been documented in this sample. Zircon occurs as sub-rounded, ~20 μm diameter grains both within the matrix and as inclusions within garnet.

Sample 89304 is from a mafic dyke that cross-cuts D₁ foliation present in surrounding felsic gneiss (Fig. 2; Hill, 1994). Sample 89304 contains the assemblage garnet + rutile + quartz + amphibole + plagioclase (symplectite) + ilmenite, with anhedral garnet occurring as a partially to completely replaced, relict phase (Fig. 3; Table 1). Zircon occurs as 50–70 μm sub-equant grains and has not been documented to occur as inclusions within garnet.

Sample 03118b is from a mafic lens hosted by felsic gneiss on Goodenough Island (Fig. 2). Sample 03118b is a partially retrogressed eclogite containing the primary assemblage garnet + omphacite + quartz + rutile and a retrograde assemblage amphibole + plagioclase (Fig. 3; Table 1). Garnet is relict and is partially replaced by amphibole. No amphibole or plagioclase grains occur as inclusions within garnet. Omphacite occurs as relict grains partially replaced by amphibole within the matrix and also occurs as rare inclusions within garnet. Rounded, equant and relatively small zircon grains (< 20 μm) occur both in the matrix and as inclusions within garnet.

APPENDIX 2: ION MICROPROBE ANALYTICAL METHODS

In situ ion microprobe $^{238}\text{U}/^{206}\text{Pb}$ dating of zircon was conducted at the University of California Los Angeles (UCLA) Department of Earth and Space Sciences Secondary Ionization Mass Spectrometry laboratory, using a Cameca ims 1270 high resolution, high sensitivity ion microprobe. The mass resolution (~4500) was sufficient to resolve mass interferences within the mass range analysed. Analyses used a 12.5 kV primary beam $^{16}\text{O}^-$ beam with ~20 nA current and ~25 μm diameter beam diameter for ablation of sample material. Portions of thin sections and standard zircon AS3 grains were mounted in epoxy. Mounts were cleaned with dilute HCl, polished and coated with a ~30 nm Au film. Intensities of monatomic U^+ , Th^+ and Pb^+ ions and $^{94}\text{Zr}_2\text{O}^+$ and UO^+ molecular ions were measured with a discrete dynode electron multiplier in peak jumping mode. Analyses consisted of 15 cycles with count times ranging from 1 to 15 s depending on isotope abundances. O_2 flooding at 3×10^{-5} Torr was applied to enhance Pb yield. Data were reduced

using in house software. Due to the young age of the samples, results uncorrected for common Pb were plotted in $^{207}\text{Pb}/^{206}\text{Pb}$ v. $^{238}\text{U}/^{206}\text{Pb}$ space (Tera-Wasserburg diagram), assuming simple mixing between radiogenic and non-radiogenic common Pb for grains analysed within each sample. The best-fit linear regression (Mahon, 1996) on the Tera-Wasserburg plot for each sample defines this simple mixture, and the intersection of this line with Concordia gives the age of each sample (Figs 5 & 6; Table 1).

Trace and REE analyses were also conducted with the UCLA ims 1270 instrument. A $^{16}\text{O}^-$ primary beam current of 10–11 nA and an accelerating voltage of 10 kV were employed. Energy offsets of 100 kV were applied to minimize interference of LREE oxides on

HREE monatomic ion species. To further correct for remaining isobaric LREE oxide interferences, peak-stripping was applied using element to oxide ratios for La, Ce, Nd, Sm, Eu and Gd that were determined on interference-free REE doped glasses. Zircon and garnet concentrations were derived relative to NBS 610 standard glass concentrations (Pearce *et al.*, 1995), using intensities normalized to ^{30}Si for both zircon and garnet. Accuracy and precision was checked by repeated analysis of reference zircon 91500 (Wiedenbeck *et al.*, 2004). Beam diameter ranged from 10 to 30 μm on both grains and standard glass. Analyses consisted of 10 cycles with count times ranging from 0.5 to 10 s depending on peak intensity for each element.